An Overview of Powder Granulometry on Feedstock and Part Performance in the Selective Laser Melting Process

Jun Hao Tan[a], Wai Leong Eugene Wong[a], Kenneth William Dalgarno[b]
[a] Newcastle University Singapore, 172A Ang Mo Kio Avenue 8, Singapore 567739
[b] School of Engineering, Newcastle University, Newcastle upon Tyne, United Kingdom

Keywords: Metal Additive Manufacturing; Selective Laser Melting; Powder Processing; Powder Characteristics; Powder Granulometry

Abstract

Metal Additive Manufacturing (AM) has begun its revolution in various high value industry sectors through enabling design freedom and alleviating laborious machining operations during the production of geometrically complex components. The use of powder bed fusion (PBF) techniques such as Selective Laser Melting (SLM) also promotes material efficiency where unfused granular particles are recyclable after each forming operation in contrast to conventional subtractive methods. However, powder characteristics tend to deviate from their pre-process state following different stages of the process which could affect feedstock behaviour and final part quality. In particular, primary feedstock characteristics including granulometry and morphology must be tightly controlled due to their influence on powder flow and packing behaviour as well as other corresponding attributes which altogether affect material deposition and subsequent laser consolidation. Despite ongoing research efforts which focused strongly on driving process refinement steps to optimize the SLM process, it is also critical to understand the level of material sensitivity towards part forming due to granulometry changes and tackle various reliability as well as quality issues related to powder variation in order to further expand the industrial adoption of the metal additive technique. In this review, the current progress of Metal AM feedstock and various powder characteristics related to the Selective Laser Melting process will be addressed, with a focus on the influence of powder granulometry on feedstock and final part properties.

1.0 Introduction to Metal AM

Additive Manufacturing (AM) has observed increasing adoption from medical, aerospace and automotive industries to manufacture prototypes and functional components with complex structures while eliminating the geometrical constraints constantly faced by traditional machining techniques. AM processes were first introduced in the late 1980's as Rapid Prototyping (RP) solutions based on various layer building and material consolidation approaches to produce quick design-to-part models for visualisation and prototyping purposes. The versatile technology offers a wide range of material consolidation mechanisms including Stereolithography (SLA), Laminated Object Manufacturing (LOM), Fused Deposition Modelling (FDM), Selective Laser Sintering (SLS) and 3D Printing (3DP) which share a common working principle of Layer Manufacturing (LM) [1]. After more than two decades of AM existence, technology advancements and stringent industrial demands forced a shift in AM approach towards Rapid Manufacturing (RM) and Rapid Tooling (RT), whereby conventional RP techniques extended their capabilities to produce directly useable components with material and mechanical performance comparable to conventional manufacturing. Currently, AM technology is focused on developing practical end-use industrial applications such as injection moulding tools, dental implants and aerospace engine components. Metal AM processes are strongly targeted at achieving

these goals to produce high value components in conjunction with design flexibility, multi-material integration as well as light weighting possibilities.

Metal AM materials and classification

Powder, wire and sheet materials are various forms of feedstock utilised in metal AM processes which also differentiate the respective construction behaviours and material binding modes of the commercialised techniques (Refer to Figure 1). Majority of the metal AM processes consist of powder-based systems including Powder Bed Fusion (PBF), Direct Energy Deposition (DED) and Binder Jetting which utilise granular powder as the primary source of material during part forming. Among these processes, PBF and DED techniques execute direct melting of powder materials to achieve fully dense parts using high energy sources (E.g. laser or electron beam) while Binder Jetting coagulates powder particles with adhesive agents before carrying out post sintering and secondary infiltration for part density restoration. Material depositions of powder-based methods are also dissimilar in which PBF and Binder Jetting processes involve the coating of feedstock onto a bed substrate prior to material consolidation while DED utilises a coaxial nozzle and beam to perform powder delivery and melting almost simultaneously. In particular, the class of PBF techniques including Selective Laser Melting (SLM) and Electron Beam Melting (EBM) processes are typically preferred routes for the direct fabrication of high quality metallic parts [2]. In comparison, SLM utilises an Nd: YAG fibre laser (~200-400W) under an inert gas environment (E.g. Ar or N) while EBM requires a focused electron beam (~60kW) within vacuum conditions [3]. Although both techniques are capable of producing near net shape metallic components, SLM generally manufactures higher precision parts with better as-built surface quality than EBM but often at the expense of longer build times and higher residual stresses [4]. While the primary reason could be due to the relatively finer powder sizes used in SLM, the influence of size distribution (granulometry) on the powder behaviour during process build-up and the resulting part quality remains unclear.

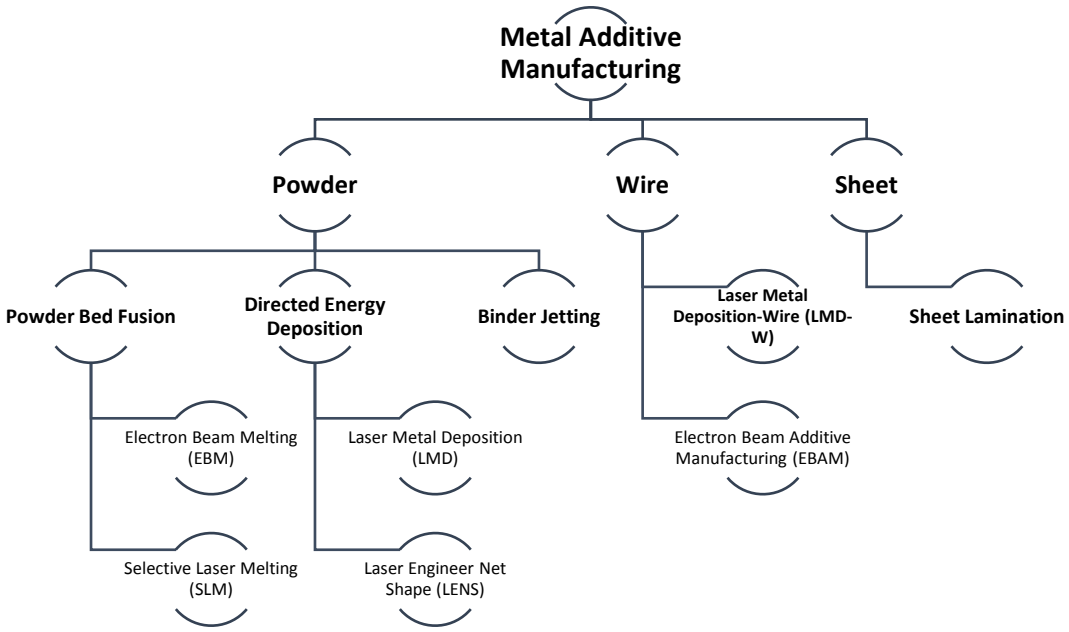

Figure 1: Metal AM processes

SLM Research

It is well known to the metal AM community that SLM technology and other PBF processes are sensitive to both process and material inputs used prior to part build-up [5]. Accordingly, many published works have concentrated on addressing the major key process parameters including laser power, scan speed, layer thickness and hatch distance which requires strategic control to generate suitable energy intensities for processing different types of metallic materials [6–8]. Existing studies

also reviewed on the mechanical properties of SLM produced parts, variations in part performance due to different orientation, build layouts, scan strategies as well as common issues and defects encountered during SLM processing which are strongly tied to its complex metallurgical phenomenon [1,9–13]. To resolve process complexity and understand the thermo-mechanical interactions occurring in SLM, numerous numerical modelling simulations and finite element approaches have also been developed and reviewed by King et al. [14]. With respect to the materials used in SLM, finer sized powders are preferred to achieve parts with better resolution when used in conjunction with reduced layer thicknesses during processing [9]. However, less emphasis was placed on the influence of powder size distribution as compared to its importance in the study of conventional sintering [15]. More recently, researchers are beginning to spend considerable efforts in quantifying feedstock performance used in metal AM which illustrated several key characteristics found in powdered materials [16,17], AM powder production methods [18] as well as metrology techniques used for AM feedstock characterisation [19,20]. However, the inter-relationships between powder size distribution (granulometry) and other material parameters (packing density, rheology, thermal properties etc.) as well as the resulting mechanical properties and microstructure of the part produced were not well understood according to the authors' knowledge.

In this paper, an overview of the SLM process as well as its existing issues encountered during part build-up will be first addressed. Next, the current progress of metal AM powder including various powder attributes and their individual influence on the SLM process will be covered. Lastly, the effects of powder granulometry changes on the powder performance and part performance will be discussed.

2.0 Selective Laser Melting

2.1 Process Description

With increasing needs to produce industrial grade metallic parts using AM technology, SLM was developed under the RM/RT approach in year 2000 to evolve consolidation capabilities from previous prototyping systems. Similar to many AM methodologies, the SLM process extracts design information from a three-dimensional CAD/STL file which is digitally converted and sliced into thin geometrical layers by a computer software. A mirror-guided laser source then scans the powder bed within an inert gas build chamber, selectively melting targeted areas on the surface of the powder bed before descending the build platform along the Z-axis at a pre-allocated thickness for the next deposition to occur. The process requires initial powder layers to be fused onto a base substrate, initially levelled on the build platform, before subsequent powder layers can be sequentially stacked upon solidified layers until the final part is completed. SLM technology uses a high-powered laser which directly melts powder particles to the molten state and produce near dense parts without lengthy post treatments like secondary infiltration as seen in SLS systems. Nevertheless, minimal stress relieving heat treatments and surface finishing operations may still be required to optimise part functionality. Furthermore, part optimisation in SLM often requires the control of key process parameters including (1) Laser Power, (2) Scan Speed, (3) Hatch Spacing and (4) Layer thickness which generates an energy density, E (J/mm^3) governed by Equation 1 [21]:

$$\boldsymbol{E = \frac{P}{v * h * t}} \tag{1}$$

Where P (W) is the laser power used, v (mm/s) represents the scanning velocity, h (μm) refers to the hatch spacing between scanned tracks and t (μm) is the thickness set to lower the build platform by a single layer during the process. Table 1 shows a list of energy density values used for producing high quality parts for common metallic materials such as stainless steel 316L. The energy density used for different material types and machines would also vary drastically due to the different material thermal history as well as the irradiation source used to generate parts. Meanwhile, SLM is still a challenging consolidation technique which limits its suitability to a narrow range of common structural alloys including steel [22], titanium [23], aluminium [24] and nickel [25].

Table 1: SLM Process parameters for stainless steel 316L

Power (W)	Scan Speed (mm/s)	Layer thickness (µm)	Hatch Spacing (µm)	Energy Density (J/$\mathbf{mm^3}$)	Ref.
180	278	50	124	104.52	[26]
380	625 - 3000	50	25 - 120	98.7 - 108.57	[27]
300	700 - 1200	30	80	104 – 178.57	[28]

2.2 Metallurgical Principle

Material consolidation in the SLM process differs from conventional casting operations where the melting-solidification mechanism depends heavily on rapid temperature changes, gravitational effects and melt convection without external pressure application [13]. Figure 2 shows the thermo-mechanical reactions which occur in a typical SLM process as the laser beam passes and strikes onto the powder particles deposited during layer build-up. High thermal irradiation energy generated by the laser source is rapidly absorbed by the exposed powder particles through bulk coupling and powder coupling means [29] which subsequently melts and creates a half segmental molten metal pool. Under Marangoni convection, surface tension gradients of the melt pool drives thermo-capillary motion according to localised temperature difference where liquid at the centre of the melt pool closest to the beam spot (hotter region) will be transported to the melt edges (cooler region) [30,31]. Since the melt pool effectively flows away from the laser beam, it exhibits a negative surface tension gradient which generates a shallow and well-distributed liquid mass. Subsequently, the segregated liquid at molten pool boundaries would gather sufficient amount of surface energy which then flows back to the heated region and completes the convection loop [30]. Under this thermo-capillary action, the molten metal further traverses through the bed of powder particles to join the pre-consolidated underlying layer and solidifies rapidly under cooling rates of about $10^6 K/s$ [32].

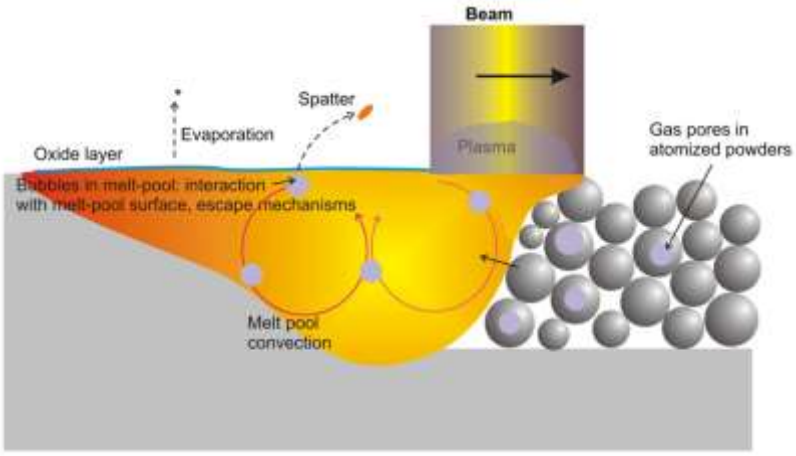

Figure 2: Marangoni Convection [10]

2.3 Existing Issues in Selective Laser Melting Process

Despite the benefits of flexible manufacturing, SLM still remains a complex metallurgical process subjected to various defects and issues related to process or material changes which significantly affect resultant build quality of the part.

Residual Stresses

The higher irradiation energy used in SLM creates steeper thermal gradients as compared to SLS which increases residual stress accumulation during part forming that propagates over multiple built layers and may result in severe thermal deformations, delamination or distortions such as part warping (refer to Figure 3). Rapid melting and solidification cycles in SLM introduce large thermal fluctuations across the solidified material during built-up which influence both compressive and tensile conditions. Two main thermal mechanisms are involved in the build-up of residual stresses during the SLM process: (1) Temperature Gradient Mechanism (TGM) and (2) Cool-down phase [33]. Based on TGM, the pre-solidified material underneath the melted layer is heated up rapidly upon laser irradiation, which readily expands but is constricted by the cold and rigid portions of the solidified piece. The restriction in thermal expansion at the local irradiated zone may generate a residual compressive stress which induces plastic deformation and possible cracking if the stress level exceeds the allowable yield strength of the material (refer to Figure 4). In the cool-down phase, the melted layer cools and contracts with a shrinkage action that is again inhibited by the underlying layer, causing tensile stresses at the upper region and compression at the bottom zone. Hence, both cyclic expansion and contraction under intermittent laser interaction results in residual stress accumulation and the largest tensile stress was often observed at the surface of the final deposited layer which could exceed the yield point of the parent material according to previous studies [13,34,35]. Researchers have also developed stress prediction tools [33,36], process refinement methods [37,38] and scanning strategies [33] to address part distortion issues due to thermal deformations in order to minimise the amount of residual stress induced in SLM components.

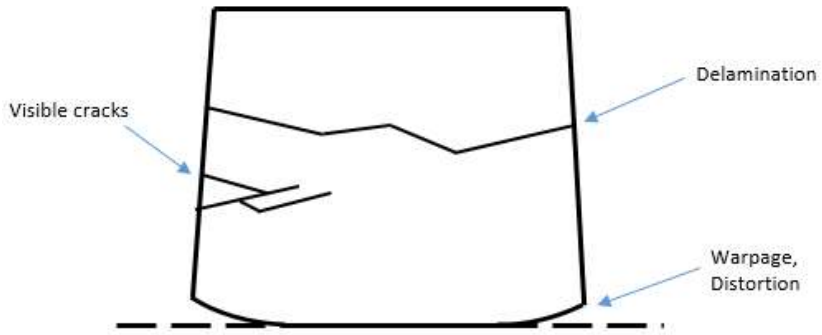

Figure 3: Possible part failures due to residual stresses

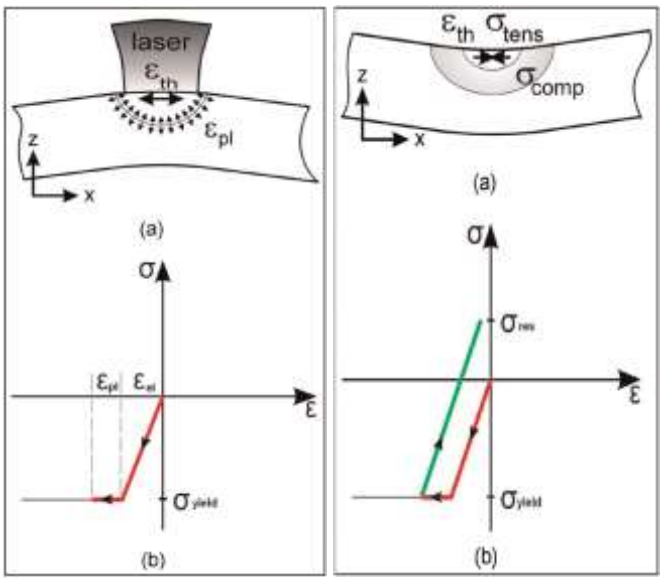

Figure 4: (left) Temperature Gradient Mechanism (right) Cool-down phase [39]

Balling

Balling is a common defect found in SLM processes which disrupts inter-layer bonding, induces porosity and degrades the surface quality of produced parts [40,41]. The adverse effect typically arises from the use of high scan speeds (low corresponding energy density) which produces an elongated melt pool that breaks up under Rayleigh instability to reduce surface tension, forming a series of fine metallic balls (10μm) staggered along the melt path (refer to Figure 5). Balling also occurs under insufficient laser power usage which generates limited melt formation and produces coarser sized balls (500μm) as a result of partially melted powder [41]. Additionally, interstitial constituents such as oxygen and hydrogen found on powder particle surfaces or dissolved elements circulating within the build atmosphere can disrupt melt pool surface tension which leads to balling. Such interstitial presence reverses capillary motion at the melt pool surface, forcing the flow of molten liquid inwards to the melt pool centre under a positive surface tension gradient and induces unfavourable wetting conditions upon spheriodisation [42]. Based on previous studies, laser re-melting (LSR), addition of deoxidising impurities and elevated laser power fusion have shown to minimise contamination and regulate surface tension [41,43].

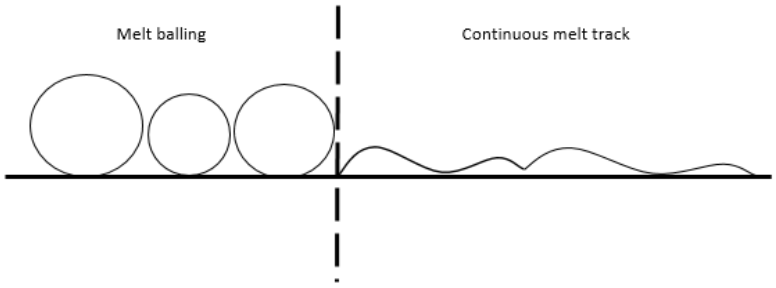

Figure 5: Balling phenomenon

Vaporisation

Laser fusion occurring at levels exceeding energy density thresholds could result in increased metal fluid evaporation beyond the material's melting point, producing metallic vapour which facilitates plasma formation [44]. The vaporisation phenomenon is commonly termed as 'keyhole mode melting' (refer to Figure 6) with deep laser beam penetration into a powder bed through vapour voids which creates a large melt pool that could also initiate balling phenomenon. For instance, overly high energy density may occur at low scan speed conditions where prolonged exposure under laser irradiation could induce boiling of the molten pool and disrupt its stability inducing small metallic balls [45]. The strong recoil pressure also introduces denudation on the powder bed together with Marangoni convection which drives the melt pool further into the powder layers creating a depression. The breakdown of the depression sidewalls upon cooling will subsequently leave entrapped irregular pores that result in poor interlayer fusion [46]. Additionally, melt spattering and ejection of low viscosity melt can also arise under rapid expansion and recoil forces during the process which degrade part surface quality and disrupt coater performance [47].

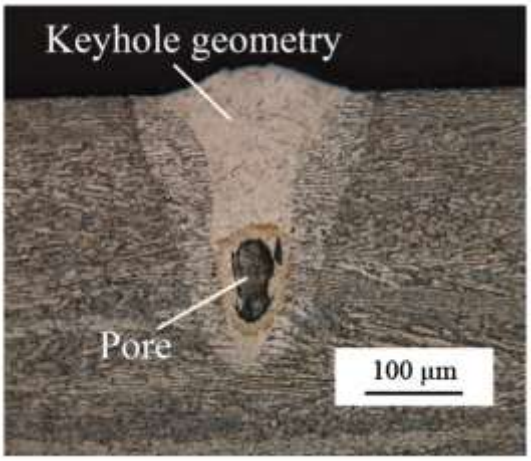

Figure 6: Key-hole mode of melting [46]

3.0 Metal AM Powder

Many high value industries are increasingly seeking to incorporate metal AM systems to their manufacturing lines in order to explore the benefits and capabilities of producing high value and complex shaped metallic components. The feedstock market is also targeted to grow exponentially together with the rise in adoption of metal AM systems including SLM and EBM where metallic powders are the main material resource for part production. Although the current metal-based AM powder market is still relatively small as compared to conventional powder processing methods such as Powder Metallurgy (PM) and Metal Injection Moulding (MIM), an increasing market trend would create more opportunities for feedstock producers to place more emphasis towards the development of refined quality powder desired for metal AM applications.

3.1 Production techniques

Although AM processes require spherically shaped powders to achieve high apparent density and smooth rheological behaviour properties during part fabrication as compared to PM and MIM, feedstock production methods are relatively similar and are shared across the metal powder forming processes. Existing powder atomisation techniques include gas, water, plasma, plasma rotating electrode, centrifugal as well as hydride-dehydride process to create useable metallic feedstock [18]. The properties of produced powder vary across the different atomisation techniques ranging from powder size, morphology, size distribution to chemical composition following the respective processing methods and atmospheric conditions used. In terms of applications, gas atomised (GA) powders are often preferred in SLM processing since they exhibit higher sphericity as compared to water atomised (WA) particles due to lower heat capacity and slower quenching rates during atomisation (refer to Figure 7). Despite the inherent irregular morphology and lower apparent density, WA powders can be used in SLM to manufacture sound parts but require process fine tuning which will be discussed further in Section 4.1. However, the high oxide content of WA grades remains a critical issue in which highly reactive metallic powders such as titanium alloys are rarely produced through this route. Instead, reactive and exotic powdered materials are sometimes produced by Plasma rotating electrode process (PREP), plasma atomisation (PA) and plasma spheriodisation techniques which promise highly spherical and purified powders [16]. Plasma processed feedstocks have also been reported to exhibit higher sphericity and uniformity in size distribution as compared to GA grades [48]. Thus, the utilisation of plasma produced powders can be mainly found in several SLM Ti6Al4V studies [23,49,50]. While better powder packing density and flow behaviours of plasma processed grades are favourable to AM processing, no distinguishable difference was noted in produced part performance over GA powders according to [51]. This may encourage consumers to stick with GA grades since plasma routes are relatively more expensive. Meanwhile, research and industry players are also studying various means

to improve the yield of spherical particles through the WA process [52–54] as well as thermal spraying methods [55] to seek cost-effective feedstock production solutions and lower the costs of AM powders.

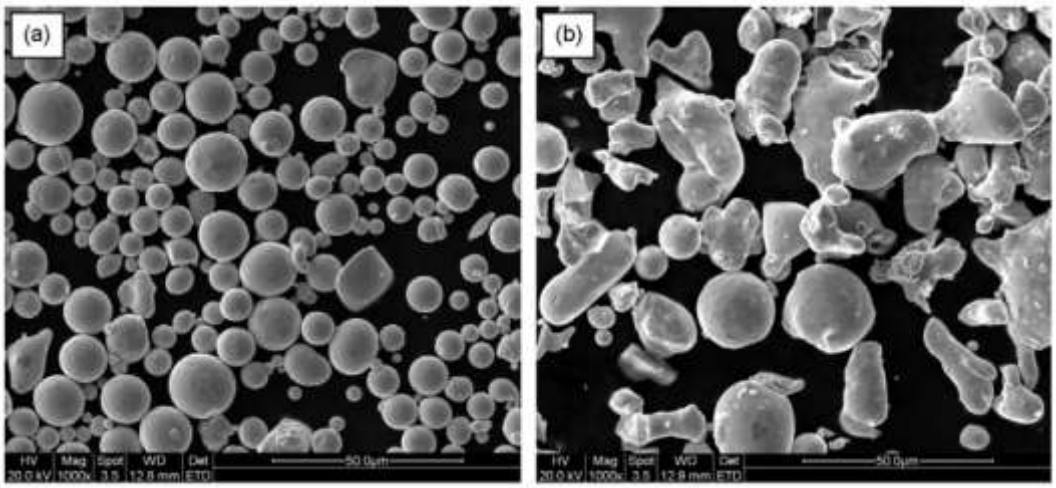

Figure 7: Gas atomised vs water atomised [56]

3.2 Commercial powder manufacturers

The existing population of AM powder manufacturers comprised mainly of machine makers (OEM), OEM-approved third party suppliers and general powder manufacturers. Machine OEMs often restrict users to a tailored range of proprietary feedstock with limited room for powder modification or extensive feedstock research and development. Alternatively, powdered materials can be purchased from external suppliers certified by OEMs but may still be relatively expensive. Nevertheless, a more cost-saving route would be the direct procurement from general powder makers but this would often require further characterisation steps before actual SLM production commences and likelihood of material inconsistency may also arise during the process. Additionally, proprietary feedstocks have designated powder attributes (size, size distribution, chemical composition etc.) which are often used within customised processes and specified material windows. Since powders are prepared differently, using a non-OEM supplied feedstock may result in less than optimum final part properties as compared to a proprietary grade. An example was found in [57] where a difference in part densification behaviour was observed between the OEM (~94-96%) and non-proprietary powder (~89-94%) despite processing under the same set of parameters, particularly under low laser power and slow scan speed conditions. Furthermore, difficulties in investigating the effects of feedstock variation on SLM processing result from a lack of open powder characterisation details which are usually undisclosed for competitive reasons, making generic powder requirements difficult to establish across all AM materials due to insufficient powder experimentation, validation and evaluation circumstances [58].

3.3 Powder Issues, Gaps and Needs

Over the recent years, many strategic efforts were mainly focused on optimising part build-up through process refinements such as increasing laser power, reducing scan velocity, hatch spacing as well as layer thickness which are well documented [26,27,59]. However, it is imperative to study the influence of various powder characteristics and establish correlations with these process windows alongside the rapid progress of metal AM [2]. Powder characteristics are often subjected to unforeseen variations over different stages of the SLM process from environmental, mechanical and thermal disturbances which affect part densification, mechanical properties, surface quality and microstructure. Large amount of research efforts have been focused on the development of suitable measurement tools and characterisation methods required for qualification and quantification of individual powder properties in order to ensure quality and consistency under repeated processing [19,60–63]. With the need to improve material efficiency through feedstock reutilisation, powder recycling techniques have also

received increasing attention to minimise contamination and other powder consistency issues which affects mechanical properties especially for chemically reactive metallic alloys [64,65]. Many physical, numerical and thermal models were also developed to break down the complexity of laser-powder interactions during the SLM process through simulated analysis but additional considerations on powder transformations from pre-process, in-process to post-process are required to validate the relationship between feedstock variation and final part properties [14]. Thus, it is important to review the influence of powder characteristics variation from the existing literature which can help to identify areas for powder material optimisation and support current thermo-mechanical simulation models to refine process prediction capabilities.

4.0 Powder Characteristics

In SLM, powder bed characteristics are governed by morphology, granulometry, surface chemistry, packing density, rheology and thermal properties which are known to affect the behaviour of feedstock and subsequent part forming procedure. Smooth flowability and high packing density of powders are some desirable attributes during SLM processing to ensure successful material deposition as well as part densification [1]. However, such parameters are also dependent on particle shape, size distribution and surface chemistry of the powder in which inter-relationships among powder characteristics exist. The following sections will address the influence of individual powder characteristics on the SLM process including brief descriptions of their respective characterisation methods.

4.1 Powder Morphology

Powders produced from different atomisation techniques will tend to vary in terms of their morphology and size which affects the packing density and flow properties of the feedstock. Highly spherical particles are often desired in the SLM process since particle shapes that conform towards unity can gradually enhance both its powder packing density and rheology performance (Refer to Figure 8 and Figure 9). Hence, qualified feedstocks typically consist mostly spherical particles with very few irregularly shaped or angular grains in its powder distribution. Powder morphology analysis commonly involves basic visual assessments of tomography and micrographs generated using optical techniques such as X-Ray Computed Tomography (CT) scans, Scanning Electron Microscopy (SEM) and Optical Microscopy (OM) respectively. Apart from spheres, other types of particle shapes (acicular, flake etc.) were previously established to describe powder geometry based on their physical features according to ASTM B243 [66]. Morphology characterisations are also performed using dimensional parameters to generate number representations for the quantification of particle geometries. The Martin's diameter, Feret's diameter and projected area diameter are various ways to determine particle dimensions based on their orthogonal distances while aspect ratio, sphericity and roundness are often used to define shape factors [20]. The aspect ratio is a simple and common approach used to perform shape analysis based on the physical measurements of powder particles including length (L), width (W) and thickness (T) where a perfect sphere approximates the condition of ($L/W = W/T = 1$) [60]. However, morphological measurements obtained through these techniques may not be reliable since they are usually derived from two-dimensional images which are insufficient to quantify the complete shape of powder particles. Nevertheless, these techniques are useful for performing quick morphology comparisons across different powder feedstocks while more subtle particle analysis requires laser diffraction and dynamic image analysis tools which will be elaborated further in Section 4.2.

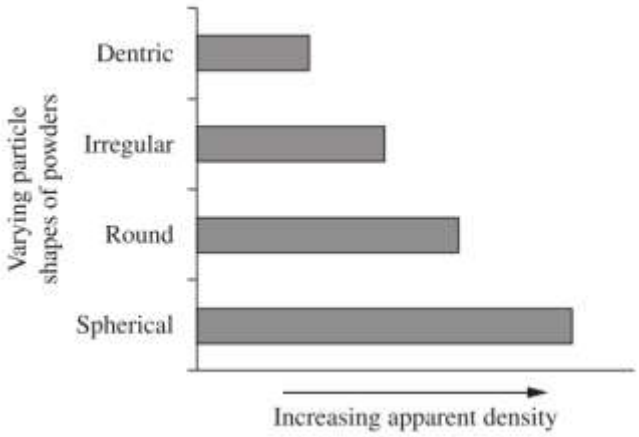

Figure 8: Powder morphology on apparent density [67]

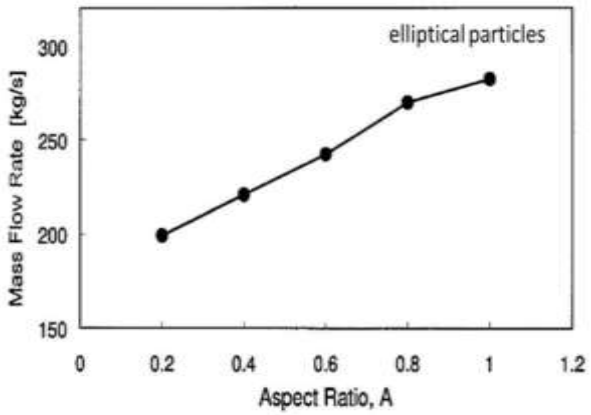

Figure 9: Particle Aspect Ratio on Mass Flow rate [68]

Since majority of the powders utilised in SLM processes are still mainly obtained from GA and WA methods, they are less spherical and contain more satellites as compared to the plasma processes (Refer to Figure 10). Formation of satellites occurs when small particles adhere to the surfaces of larger ones due to collisions during atomisation which generates an aspect ratio of ($L/W > 1$) [60]. Nevertheless, GA powders are appreciably more spherical than WA grades and exhibit smoother particle surfaces which facilitates inter-particle motion to provide better powder packing ability [69,70]. The difference in particle morphology also lead to larger pore sizes (Refer to Figure 11) and higher porosity found in parts produced by WA feedstock as compared to GA due to poor packing behaviour [56]. However, Irrinki et al. [71] recently reported comparable part densifications (96 - 97.5%) achieved by both types of atomised powder when laser consolidation took place at an energy density of $104 J/mm^3$. Although GA powder produced denser specimens than the WA grade at lower energy density levels (64 – $84 J/mm^3$), part density was observed to be independent of powder morphology when an appropriate energy density ($\geq 104 J/mm^3$) was used. However, the high content of interstitial elements present in WA powder which accelerates oxide formation would be the main concern when selecting suitable material feedstock. Based on the literature, powder morphology mainly addresses the dimensional and physical aspects of powder particles produced from different types of atomisation techniques. As far as ensuring optimum flow and powder packing efficiency is concerned, further understanding of particle size distribution and surface chemistry is required which will be discussed in the upcoming sections.

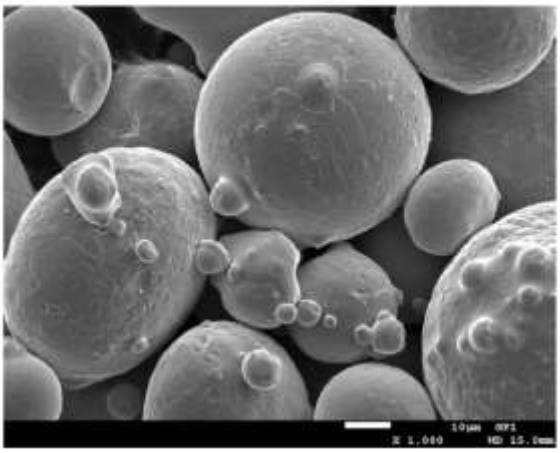

Figure 10: Formation of satellites on particle surfaces [60]

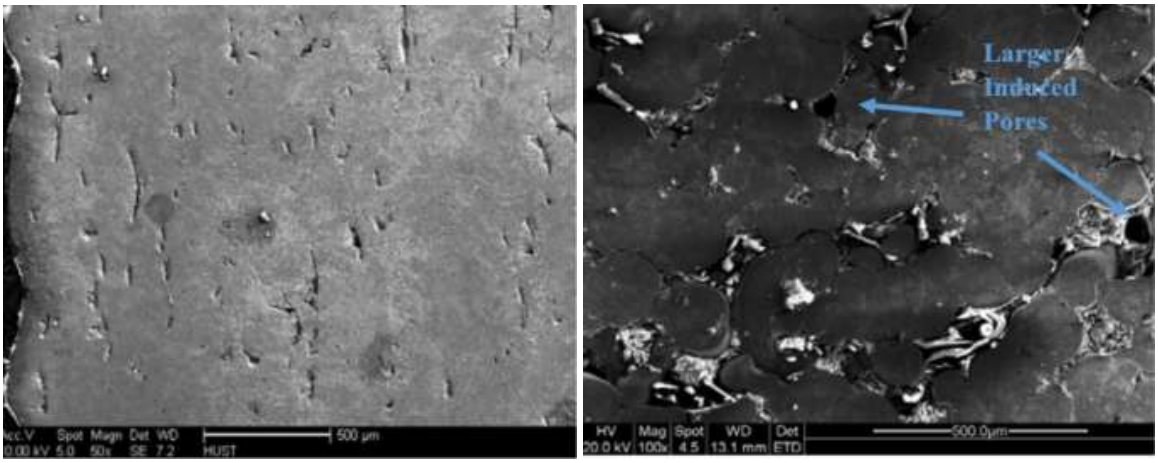

Figure 11: Micrograph of SLM parts produced from Gas atomised (left) and Water atomised (right) [56]

4.2 Powder Granulometry

While powder morphology reveals the aesthetic structure of powder particles, the granulometry or size distribution (PSD) is commonly used to quantify particle sizes in terms of volume composition. PSD is a highly dynamic parameter which fluctuates over various stages of the SLM process including powder storage, spreading as well as recycling, subsequently inducing variations in feedstock behaviour [10]. Granulometry changes are mostly observed in recycled powders that contain particles larger than the coated layer thickness due to segregation from the build compound via the feeder device which shifts the distribution curve to coarser sized regions (See Figure 12) [63,65]. Powder coarsening could also arise from pre-sintering of particles near the melting zone where droplets of molten metal ejected from the melt pool may adhere onto unfused particles, forming larger and less spherical powder structures. While the PSD difference between fresh and recycled powder is usually below 10%, increase in powder aggregation with higher number of build cycles (See Figure 13) could disrupt flow and packing performance for subsequent forming operations [60]. As such, necessary sieving procedures prior to reutilisation of the used feedstock are performed during powder recycling operations in order to minimise size deviations from the original particle distribution array.

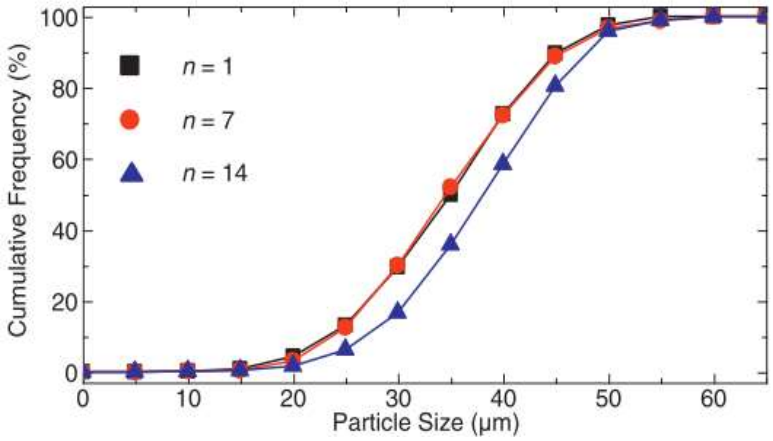

Figure 12: Coarsening of PSD after IN718 powder reuse [65]

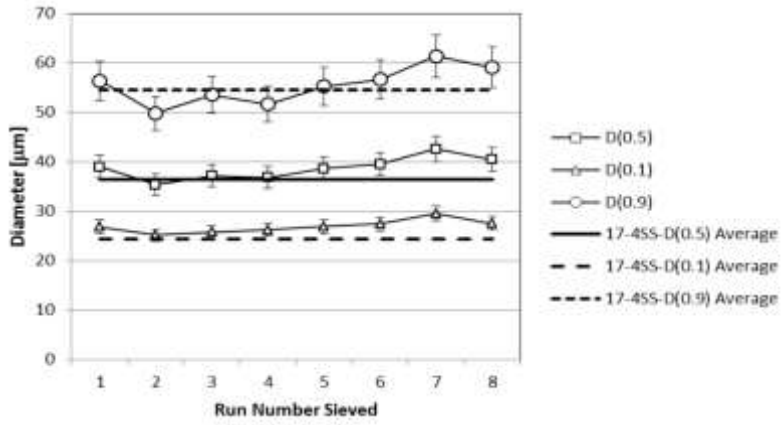

Figure 13: D_{10}, D_{50} and D_{90} increase with number of build runs [60]

Many commercial feedstocks used in SLM processes follow a *Gaussian* distribution whilst the addition or removal of powder particles through mixing and sieving operations could substantially affect the behaviour of the distribution curve resulting in other model variants as shown in Figure 14. In *Gaussian* (normal) distributions, the mode, mean and median coincides at a single central tendency of the curve while negatively and positively skewed distributions are asymmetrical as a result of higher fractions in coarse and fine particles respectively. On the other hand, multimodal distributions will exhibit two or more distinct peaks at discrete particle sizes which indicate the respective modes of the distribution. While features on a size distribution curve provide qualitative indications of the overall powder behaviour, various techniques such as sieving, laser diffraction and dynamic image analysis are required to characterise the volume of measured particle sizes through shape detection and size screening procedures. Sieve analysis provides a simple approach to derive the PSD by displacing powder samples through a series of stacked sieves in descending order of mesh sizes subjected to mechanical vibration according to ASTM B214 [72]. Subsequently, each distinct mesh (n) will retain particles which are impenetrable to the next mesh (n + 1), thus generating a spectrum of particle sizes collated into a PSD. However, very narrow bin sizes between adjacent meshes are often required to produce accurate PSD results which incur high costs and time-consuming measurements. On the other hand, the laser diffraction method is more popularly used as large number of measurements can be obtained within shorter timeframes and repeatable results are ensured through proper sample dispersion following ASTM B822 [73]. During measurement, the technique captures diffracted rays formed by individual powder particles subjected to electromagnetic impingement while background algorithms (Mie Theory, Fraunhofer Theory etc.) analyse and condense the scattered pattern into a PSD spectrum [74]. Although the process can provide accurate PSD measurements for most powder-based AM processes which often

utilise highly spherical powders, certain unreliability arises when examining irregularly shaped particles. Due to the assumption of perfect spheres during particle analysis, the scattering pattern and dimensions of non-spherical powders can only be approximated [60]. Nevertheless, existing image based analytical tools may overcome such challenges through inspecting powder shapes performed in accordance to ISO 13322 [75]. High-resolution static image analysis instruments (E.g. Morphologi G3) capture the optical images of detected powder particles and subsequently match morphology indexes against its database containing various particle shapes to derive shape attributes (Circularity, convexity, elongation etc.). Powder sizes are derived through translating the projected area of each captured particle to an equivalent sphere having distinct diameter, thus generating a spectrum of circle equivalence (CE) diameter as well as sphere equivalent (SE) volume figures for PSD analysis [76]. Alternatively, studies have also used dynamic image analysis (DIA) tools (E.g. Camsizer X2) in which the silhouettes of falling powder particles from a vibratory hopper are instantaneously captured within a measuring space region established between a pulsed light source and dual cameras [63]. The use of two cameras helps to improve accuracy in image capturing by each focusing on large and small particles respectively at different magnifications [77]. Overall, image analysis methods may offer higher resolution over non-image based techniques through direct physical measurements especially when examining feedstocks with high amount of fine satellites and/or irregular particles such as WA grades.

PSD results are usually presented in a differential curve to distinguish the mode, mean and median particle sizes of the feedstock and a cumulative graph which identifies the volume content in terms of size gauges (D_{10}, D_{50} and D_{90}). Using Figure 15 as an example, $D_{10} = 20\mu m$ indicates that 10% of the powder sample is less than $20\mu m$; $D_{50} = 45\mu m$ represents the median value and specifies that 50% of the powder is below $45\mu m$; and $D_{90} = 60\mu m$ depicts that 90% of the particles are smaller than this size. Additionally, distribution widths can be obtained through standard deviation measurements from the central tendency while the span ($\frac{D_{90}-D_{10}}{D_{50}}$) is sometimes used to represent the width of a *Gaussian* size distribution based on size metrics computation [78]. However, different measurement approaches such as the size width ($2.56/log_{10}(D_{90}/D_{10})$) may be employed when comparing different types of size distributions (E.g. *Gaussian* vs multimodal) [71]. Typically, a higher standard deviation, larger span or size width are common indicators of a wider distributed powder and vice-versa. Various size distribution models were also previously known to produce different packing behaviours which affect shrinkage and densification of forming parts in conventional sintering processes [15]. In a similar manner, the study of granulometry variation could receive new interests in the SLM process as well as other powder-based AM techniques since changes in powder size characteristics can influence material process-ability throughout the entire process build-up. Existing works have also established preliminary powder granulometry requirements suitable for SLS and SLM processes including $D_{90}/D_{10} \leq 19$, $D_{50}/D_{10} \geq 10$ and $D_{90} < t_{layer}$ [69,79]. As such, the size metrics and distribution model representations will be used to describe the effects of powder size distribution on powder and part performance in this review.

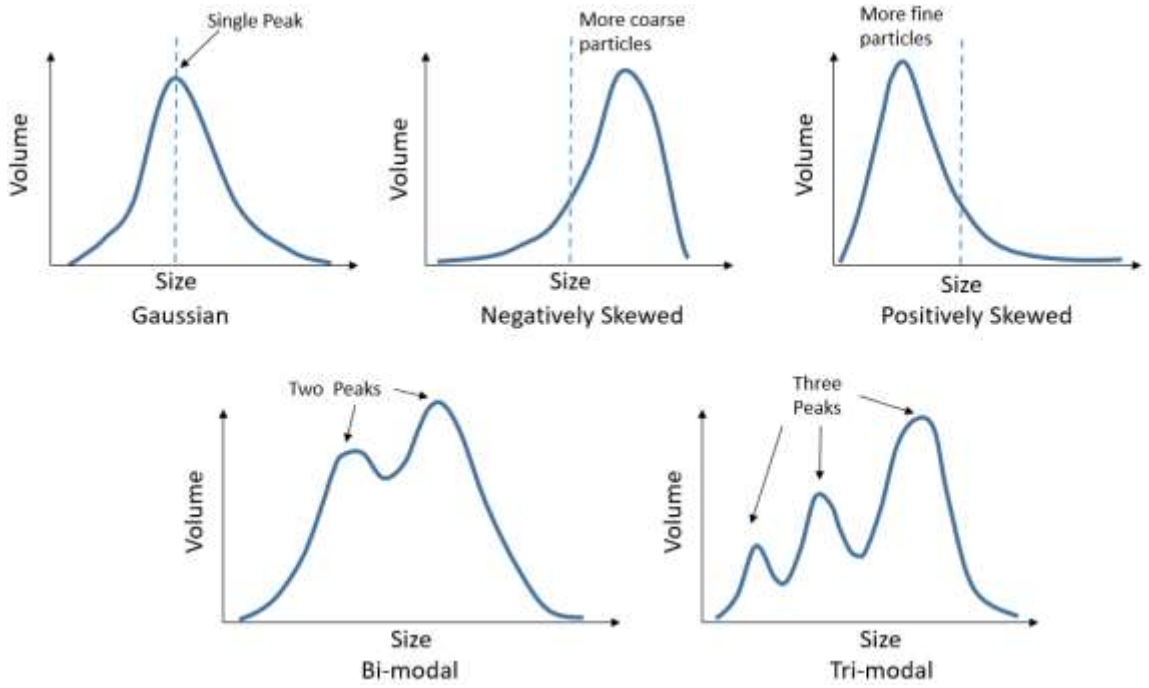

Figure 14: Variations of Powder Size Distribution

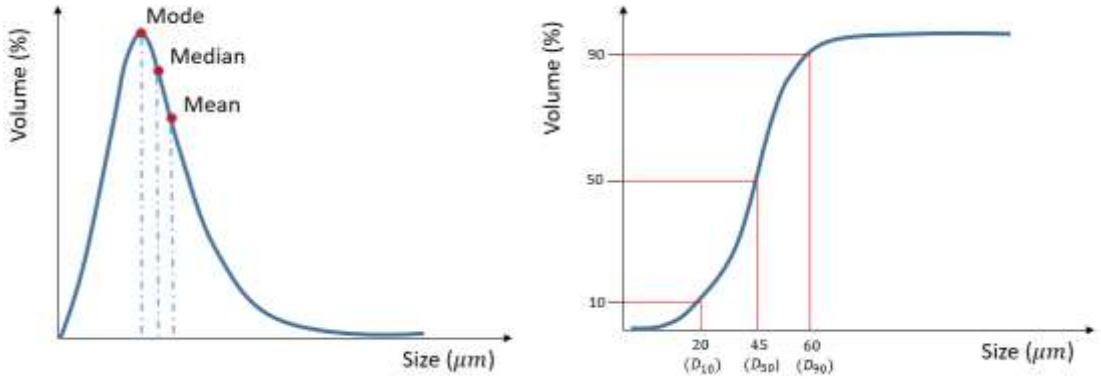

Figure 15: Differential (left) and Cumulative (right) Size Distribution

4.3 Powder Surface Chemistry

Powder contamination has been an underlying issue in SLM especially during the processing of highly reactive feedstock such as magnesium [80], titanium and aluminium alloys [81]. Prolonged exposure of reactive feedstock to external environments, interstitial gas intrusions and the close proximity to heat irradiation during part forming would trigger oxidation reactions [10,82]. Oxidation hinders part consolidation through the formation of oxide skins on powder surfaces which translates into the molten pool upon melting, causing instability that breaks up the melt pool into droplets known as the balling effect covered earlier in Section 2.3. Additionally, hardened oxide films also hinder proper surface wetting conditions which subsequently generate poor adherence across formed layers that induce part porosity [40]. Another mode of contamination refers to the formation of hydroxides due to moisture adsorption at powder surfaces which occurs under relatively high humidity conditions [83]. As compared to solidified oxide layers which are often hard and brittle, adsorbate films exhibit a viscous behaviour which disrupt the flow of particles within the powder bed due to an increased tendency of agglomeration [84]. Furthermore, the drop in water vapour pressure at elevated build chamber temperatures could trigger hydroxide layers to produce oxides upon crystallisation which can further

degrade the build chamber atmosphere. Irradiation contact with adsorbed water layers would also facilitate the dissociation of hydrogen atoms from water molecules during laser-powder interaction which can produce entrapped gas pores upon melt pool solidification that contribute towards melt pool spattering [10]. X-Ray Photoelectron Spectroscopy (XPS) is often used to analyse the concentration of elemental constituents through beam probing on the surface of powder particles and detect the presence of interstitial inclusions. Chemical element identifications are based on the energy peaks recorded through the kinetic motion of electrons subjected to irradiated excitation at the surface layers (0-10nm). Additionally, moisture analysers can be used to monitor the humidity content of prepared feedstocks as shown in a particular study [85] where starting powders were preheated (E.g. 80℃) until a low relative humidity level (<0.01%) was reached prior to SLM processing. Based on a thermogravimetric method, moisture analysis requires powder samples to be weighed before and after drying at elevated temperatures while moisture content is computed based on the weight differences. In conjunction with moisture analysers, humidity sensors may be used to ensure stored powders are kept at low moisture conditions. It would also be useful to study the surface free energy of powder particles associated with surface chemistry changes (E.g. moisture contamination) through techniques including the sessile drop method, Inverse gas chromatography (IGC) as well as Atomic force microscopy (AFM) [86]. The sessile drop method probes powder particle surfaces using a wetting liquid with known surface tension and derives surface free energy of the solid particle using Young's equation [87]. On the other hand, IGC uses a gas displacement strategy conceptually similar to the Brunauer, Emmett and Teller (BET) method for powder surface area measurements which will be elaborated further in Section 5.1. Last but not least, AFM is a rather expensive tool but has shown to detect presence of stronger adhesion forces with increasing relative humidity in pharmaceutical powders [88]. Subsequently, the degree of powder cohesion with varying moisture content can also be characterised using various powder flowability measurements found in Section 4.5.

Although the SLM process is often performed under controlled inert conditions (O_2<0.15%), oxygen pick-ups and inclusions are still unavoidable, especially in chemically reactive powder materials [63]. Excessive oxide content can cause degradation in mechanical properties such as embrittlement to structural alloys [89]. Besides particle shape irregularity, high amount of surface oxide content has also shown to degrade powder flowability [67]. It is therefore appropriate to study the effects of powder contamination on parts generated under different feedstock conditions by measuring the change in oxide levels between starting and recycled powder. The oxygen content in recycled Ti6Al4V powder was found to rise above 50% of its original composition which resulted in a 14% decrease of overall part toughness [63]. The reduction in ductility was also accompanied with part porosity increase from 0.17% to 0.36% following powder re-usage. However, the degree of oxidation in recycled feedstock was found to be less severe in a similar study by Ardila et al. [65] whom observed slight loss of Ni content (52.1 Wt.% to 51.5 Wt.%) in IN718 powders subjected to oxidation (Refer to Figure 16). It could be due to the different powder recycling methodology used where [63] only performed sieving procedures before blending it with 5% new powder while [65] carried out an additional drying operation before reutilisation. The drying step could have aided residual moisture removal in used powders which was also reported to reduce porosity in SLM Al-12Si parts (Refer to Figure 17) caused by oxide and hydroxide formation elsewhere [90]. A similar surface conditioning approach was also performed on Ti6Al7Nb powder to improve its flowability [91]. Other studies have explored the addition of inhibitors to curb oxidation issues during melt pool formation in SLM [31,92,93]. The addition of phosphorus, carbon and graphite to iron-based alloys were reported to provide deoxidising effects which helped to reduce the surface tension of the melt pool, preventing balling occurrences. Such deoxidising treatments could also be integrated to powder recycling solutions and refine the quality of recycled feedstock. However, the severity of contamination with compounding build cycles requires further investigation especially when interstitial attack is strongly prevalent in highly reactive alloyed powders [94]. Furthermore, the risk of powder contamination could also be linked to effects of surface area which

depends on the particle size and size distribution, less studied in the literature but should present potential impacts on contamination at powder surfaces which will be discussed in Section 5.1.

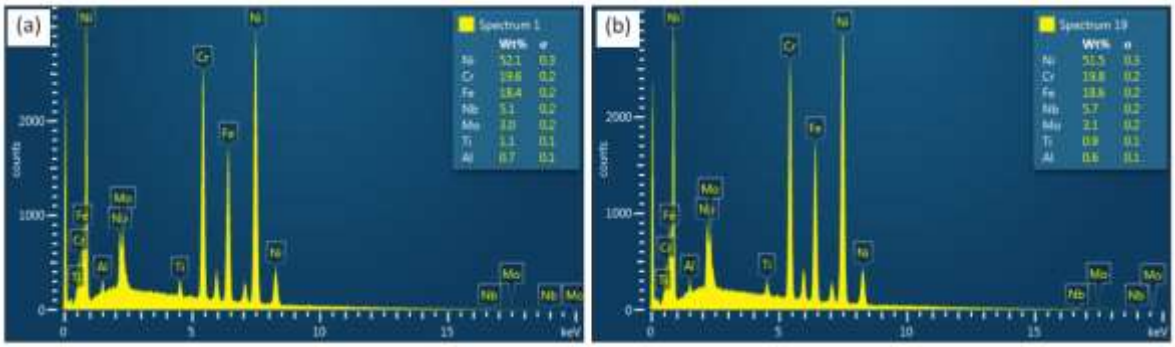

Figure 16: Difference in Chemical Composition of IN718 Powder between 1st build (left) and 19th build (right) [65]

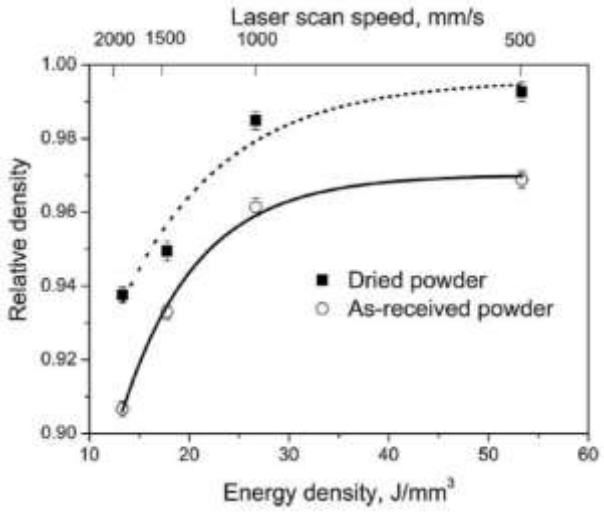

Figure 17: Dried Al-Si12 powder vs As-received Al-Si12 powder [90]

4.4 Powder Packing Density

Powder packing density, also known as fractional density, is a crucial feedstock parameter which determines how efficient powder particles are able to arrange themselves with maximum particle-to-particle contact and minimum voids within the granular network. There are several key factors which affect particle packing behaviour including size distribution, morphology, inter-particle forces, surface chemistry as well as flowability [95]. Actual powders often do not mirror the close-packed behaviour of uniform and equivalent-sized spheres found in face-cubic-centred (FCC) and hexagonal-close-packed (HCP) systems. Instead, they are loosely arranged in a poly-dispersed manner with a mixture of random particle sizes as well as an arbitrary order of interstitial pore distribution, leading to relative packing densities ($p_{relative} = \frac{p_{powder}}{p_{bulk}}$) about 40-60% of parent material. Interfacial voids may also arise at disconnections between the powder and container interface known as 'wall effects' but were said to be negligible in SLS and SLM processes since the rough surfaces of solidified layers allow newly coated particles to reside into the voids [69]. Furthermore, it is important to note that coating faults can also disrupt the local effective packing density of the deposited powder layer prior to laser absorption (Refer to Figure 18). Non-uniform packing properties across a powder layer will consequently produce inconsistent exposure of powder particles under the irradiation source at different locations which could lead to inhomogeneous material coalescence. During solidification, powder layers experience a shrinkage along the build direction (Z-axis) in the first few depositions when they are fused to nearly full material density (E.g. from 60% to 99%). Increasingly porous powder layers will require a longer

transient period (higher number of layer depositions) before reaching a stable effective layer thickness (Refer to Figure 19) [58]. Subsequently, a larger amount of porosity in powder layers could induce higher shrinkage of melt pools between 21 to 54% according to [96]. Although inaccuracy at the starting layers may only disrupt the construction of support structures which will subsequently be removed from the actual part, it is important to consider the trailing effect if no support structures were to be employed. Following process build-up, powder layers also gradually translate into a powder bed which provides support for the forming component and act as a secondary heat sink to prevent thermal defects wherein both cases, optimal powder packing behaviour is required [97]. In addition, high powder packing density is always desired which increases the part density of formed materials (Refer to Figure 20) [67].

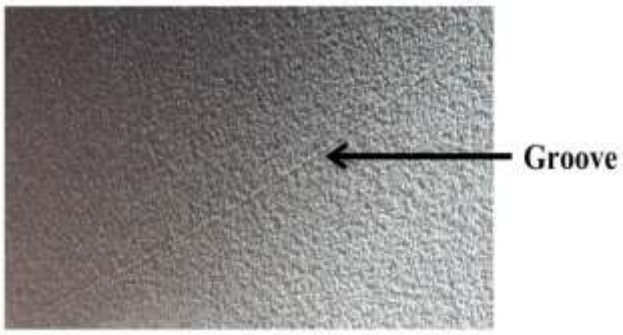

Figure 18: Coating defect in SLM process [96]

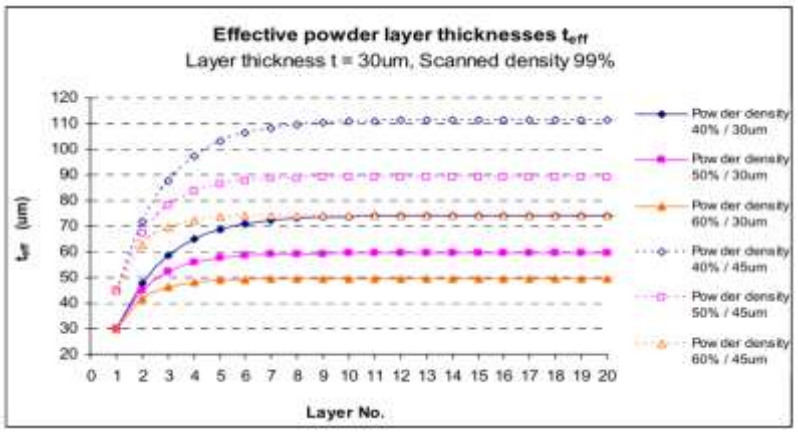

Figure 19: Effective powder layer thicknesses of different powder packing density [58]

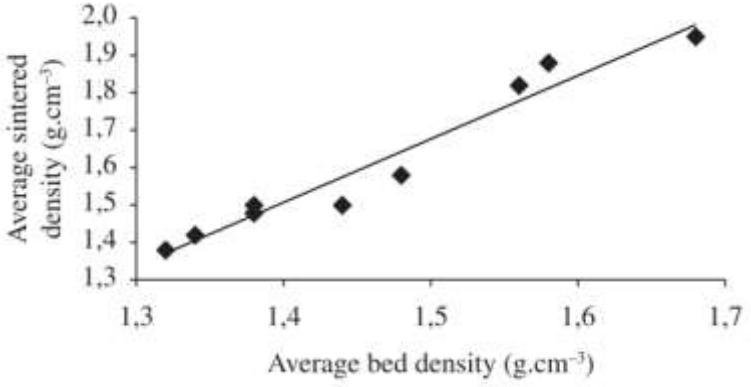

Figure 20: Average Bed Density Vs Average Sintering Density [67]

To detect changes in packing density of the powder bed, visual tools such as camera imaging and SEM are not entirely suitable due to the lack of resolution to observe particle-scale motion and feasibility

issues respectively. Due to the complexity in monitoring powder bed activity, numerical models were developed and used to investigate laser-powder interactions and study the dynamic changes of the process [14,98]. Process simulations would also require intuitive modelling of the powder bed to obtain a stochastic powder packing behaviour that highly resembles commercial feedstock. The Rain model [99] and Discrete Element Method (DEM) [100] are some examples used to construct a powder bed through random particles' allocation with the integration of commercial powder attributes including particle size, size distribution and packing density. Existing simulation studies for SLM have shown that poor powder packing density disrupts melt pool stability where balling effects were said to arise at porous sites that can result in defective parts [96,100,101]. Figure 21 also shows the stabilisation of melt pool when powder packing density was increased from 38% to 45% which inhibited balling defects by forming a continuous melt pool, preventing fluid instabilities (downward flow) caused by gravitational forces [100].

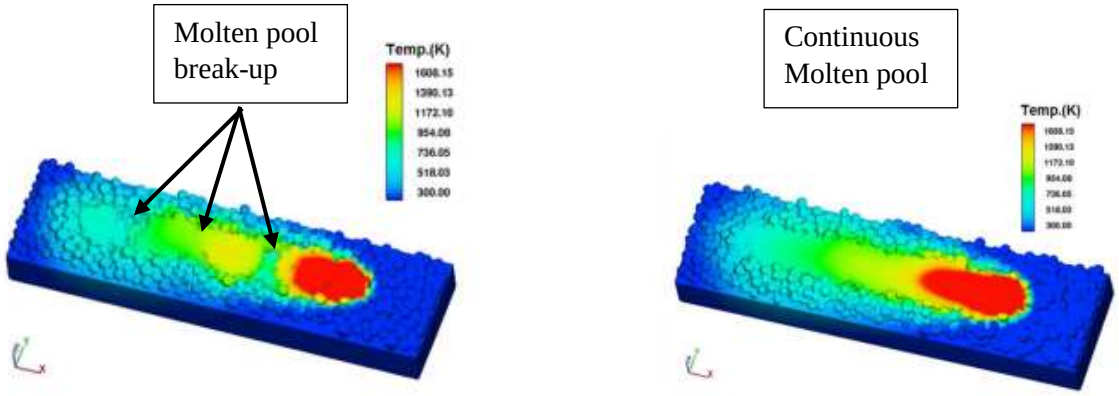

Figure 21: Melting of powder layer with 38% (left) and 45% (right) packing density [100]

The evaluation of powder bed density could also raise another metrology challenge to researchers as different types of measurement techniques were practised across existing studies, resulting in a variety of powder bed density (PBD) representations. Tapped and apparent densities used to describe the dense and loose random packing of powder particles respectively are obtained from Hall flow, Carney flow, Scott flow and Arnold flow techniques but may not provide the best indicators of packing density. Recently, NIST researchers developed a suitable cylindrical specimen to perform in-situ PBD measurements for PBF processes [102]. The hollow specimen consisted of a shelled interior which concurrently collects the coated powder as its exterior structure is being built. The design is believed to be an improved version from earlier studies [69,85,103,104] which introduced an enclosed lid to prevent powder spillage and was able to detect subtle changes in PBD across the powder bed. Existing studies have also compared PBD values obtained from the in-situ method which found to saturate between tapped and apparent densities [85,104] While such measurements can be time-consuming and often at the expense of powder material as compared to conventional tapped and apparent density evaluations, the approach may more accurately portray the packing behaviour of feedstocks used in PBF processes since powders are assessed in as-coated conditions rather than pre-deposition states. Additional efforts should however be paid on applicability of the measurement technique for powders with different atomised natures [104]. Meanwhile, other metal AM processes such as DED may still rely on conventional methods in the absence of a coated powder bed and employ the tap density method which is believed to mimicking feedstock delivery from a vibrating hopper [105]. Furthermore, intricate measurements may be obtained at single powder layers but demands greater effort since powder sizes typically used in laser consolidation processes are comparable with the layer deposition thickness (micro-scale) used to contain those particles. Extensive design of experiment studies are also required

to study the evolution of powder packing behaviour from a single powder layer to multiple layers as well as the overall powder bed together with the effects on part forming at different powder scales.

4.5 Powder Flowability

Good powder flowability is essential in SLM processes as granular feedstock needs to be smoothly coated across the build area and create a homogenous powder layer prior to laser consolidation. Powders with high cohesiveness would induce difficulty during powder spreading and generate inhomogeneous regions which subsequently affect its packing density, thermal and optical properties [62]. Powder cohesivity is dependent on its inter-particle forces (F_i) and particle weight (mg) according to the granular bond ratio ($BN = F_i/\text{mg}$) previously defined by [106]. Fine powders (high BN) will generally possess a higher tendency towards cohesion and agglomeration due to stronger inter-particle attractive forces (E.g. Van der Waals) as compared to coarse powders (low BN) [107,108]. Nevertheless, they are still largely utilised in SLM systems since small layer thicknesses (E.g. 30µm for SS 316L parts) are usually recommended in process windows to achieve optimum results and produce higher resolution parts [57,58,109].

By far, simple flow measurements such as Hausner Ratio (HR) and Angle of Repose (AOR) are widely used to determine the rheological behaviour of AM powders. The Hausner Ratio ($HR = P_T/P_A$) is computed using tapped (P_T) and apparent (P_A) density values obtained through a graduated cylinder according to ASTM D7481 [110]. It is a density dependent measure where HR >1.40 represents poor flowability while $HR \leq$1.25 describes a less cohesive and more free-flowing characteristic [111]. On the other hand, the angle of repose (AOR) utilises a Hall flowmeter described in ASTM B213 [112] which measures the angular difference between the slope of the accumulated powder heap and the base plate where a low angle or shorter discharge period depicts better flowability. Typically, powders which exhibit AOR values less than 30º represent good flowability while presence of powder cohesion occurs above 40º [113]. However, HR and AOR measurements may not solely adequately portray the flow behaviour of feedstock used in SLM systems and would require additional dynamic flow measurements to fully describe the rheological performance of powders distributed by a coater/feeder device [107]. Recently, a powder revolution analyser technique which measures the dynamic state of powders was studied by [62] and was said to be analogous to the delivery conditions in SLM systems. It consists of a rotating drum that illustrates powder motion under repeated roller depositions while powder images are simultaneously captured over multiple revolutions (Refer to Figure 22). In the study, *Gaussian* powders which exhibited good flow tend to possess low avalanche angles between 49~54° and a surface fractal value of ~5.0. Other rheology diagnosis tools include Ring Shear Cell [114] and Freeman FT4 Rheometer [115] which measures powder flow under torque and axial loading conditions. The rheometer is a much preferred method for evaluating powder rheology in SLM applications since flow measurements are conducted under relatively lower stress states similar to powder feeding as compared to ring shear testing which is more applicable to hoppers [116]. The technique measures Basic Flow Energy (BFE) and Specific Energy (SE) of powders which quantifies the flow resistance during constrained and unconstrained circumstances. It was also used by a commercial powder manufacturer to compare the rheological performance between new and recycled feedstock [61]. Results from the study are reproduced in Figure 23 where the flowability of used powder was observed to deteriorate after a build cycle with >33% increase in Basic Flow Energy (BFE) over the original condition due to possible agglomeration or pre-sintering effects. In order to reutilise used powder, new powder was blended to form a mixture which improved powder flowability closer to the virgin state. The decrease in flowability of recycled powders is also tied to the effects of powder size distribution coarsening mentioned in Section 4.2, where the occurrence of pre-sintering formed irregularly shaped powder clusters which increased particle size as well as induced flowability reductions. While powder flowability is clearly affected by its morphology, the review will focus on the influence of powder size distribution on rheological properties as further discussed in section 5.1.

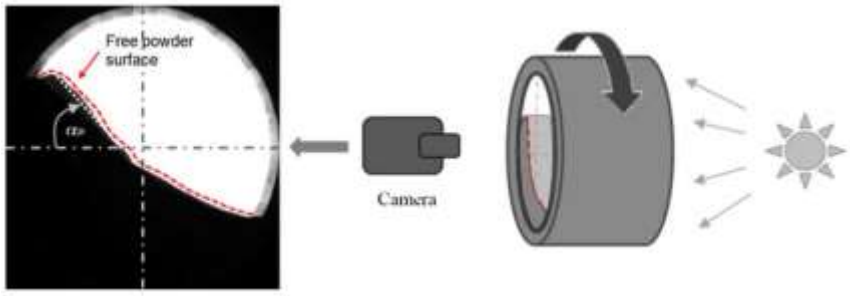

Figure 22: Illustration of Revolution powder analyser [62]

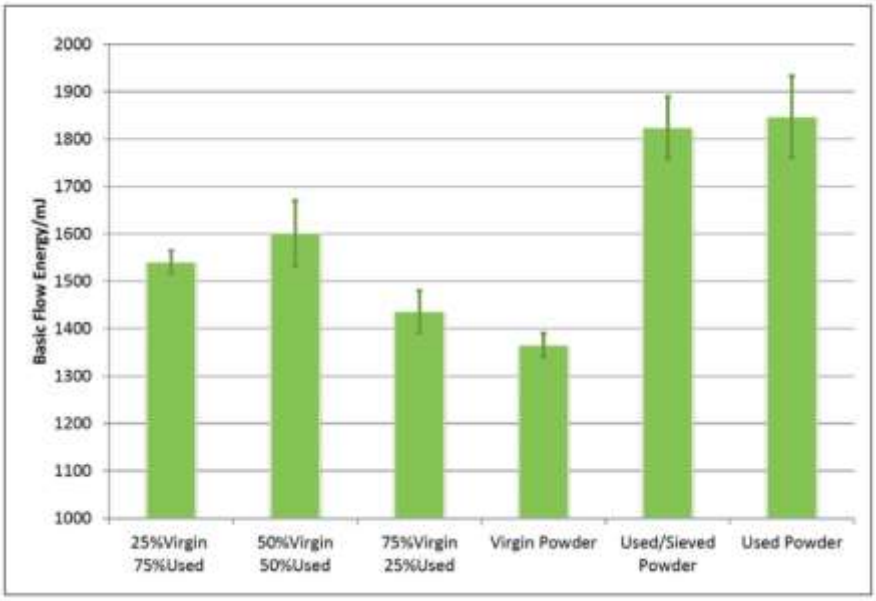

Figure 23: Flow energy of different powder conditions [61]

4.6 Powder Thermal Properties

SLM is a thermo-mechanical process which involves intensive interactions between laser source and powder bed as well as the complex heat transfer activity during part forming. Hence, powder thermal properties such as absorptivity and conductivity are crucial parameters which affect laser absorption, melt formation and other heat transfer related mechanisms in the process [117]. As compared to bulk solids, a cluster of powder particles has relatively higher absorptivity due to the inter-particle voids within loose arrangements which promote penetration of the irradiation source into the powder bed under a multiple scattering effect [29]. In other words, when a high energy laser strikes the coated powder layer, portions of the beam are divided into a spatial distribution comprising of forward/backward scattering, transmission and reflectance besides thermal absorption at the surface [118]. The magnitude of beam penetration through the powder bed is also termed as the Optical Penetration Depth (OPD) where laser intensity declines to $1/e$ (~37%) from the incident value [119,120]. While OPD only provides a qualitative measure, some studies have tried to determine the thermal absorptivity of powders with the aid of an integrating sphere [121,122]. It has been shown previously that metallic powders absorbed better under the Nd-YAG laser with a smaller wavelength ($\lambda = 1.06\mu$m) as compared to the CO_2 laser ($\lambda = 10.6\mu$m) which favoured non-metals [122]. However, such thermal absorptivity measurements were mostly complicated and expensive to replicate. Meanwhile, laser absorption simulations such as the Ray tracing model may help to predict the absorption behaviour of various powders processed under SLM but were still unable to provide accurate measurements for powder materials with high particle surface roughness and oxidised skins [123–125]. For validation purposes, a simple calorimetry method was recently proposed by [126] to carry out direct

absorptivity measurements on powder deposited in a similar manner to SLM systems with the consideration of other heat transfer effects. Powder thermal absorptivity was determined based on temperature changes over a powder-coated disk with known dimensions, under a uniform exposure of 1µm laser irradiation (Refer to Figure 24). The measured absorptivity results found good agreement with the Ray tracing model for stainless steel 316L feedstock while it was observed to be 15% higher than the predicted value when probing highly reactive powders due to the presence of surface oxides.

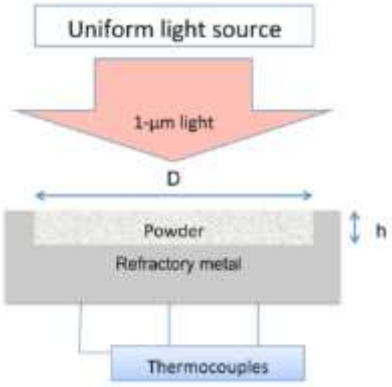

Figure 24: Illustration of Calorimetry technique [14]

In contrast to thermal absorptivity, thermal conductivity is significantly reduced in powders compared to their bulk forms since porosity limits the number of particle contacts in the powder bed. Hence, the effective thermal conductivity of powder particles is mostly controlled by the gaseous medium among the voids which varies with granulometry and packing density while less influenced by material thermal attributes. With regards to metrology, existing studies have gathered a series of techniques previously used for measuring the thermal conductivity of bulk materials which are also applicable to AM powders [20,127]. The available methods can be classified into (i) steady state: guarded hot plate, cylindrical, spherical and ellipsoidal and (ii) transient state: hot wire, thermal probe, hot strip and flash method which mostly involve contact temperature sensing and conductivity computations using heat transfer theory. The flash method also seemed to be analogous to the calorimetry method used for thermal absorptivity measurements which detect temperature changes under high energy light exposure [128,129]. In addition, researchers have develop several numerical models to simulate the heat transfer mechanisms during the SLM process in order to predict melt pool formulation as well as part consolidation which require the input of powder thermal properties [14,119,124,130]. As such, the Finite Element Method (FEM) is commonly used to study the physical changes during laser interaction and to develop different approaches for process optimization and part failure prediction such as distortion, porosity and thermal stresses. Other techniques including Lattice Boltzmann (LBM) and Finite Volume Method (FVM) were more focused on powder particle evolution of the powder bed, taking into account the melt pool hydrodynamics during laser irradiation [131]. Altogether, these simulation models demand accurate powder granulometry and morphology information to generate actual particle arrangement and modelling of initial powder packing while the understanding of powder size distribution influence on thermal properties can help to build on more robust simulations for PBF processes.

5.1 Effects of Powder Granulometry on Feedstock Performance

Based on the various powder characteristics addressed, morphology and granulometry are considered primary attributes that could affect secondary powder parameters, which jointly depict the feedstock behaviour. While studies have highlighted the clear advantages of utilising highly spherical powder particles during SLM processing, there is no optimum powder size distribution model to quantify feedstock quality in terms of size or composition ratio between coarse and fine particles. Hence, the

following sections will discuss on the influence of powder granulometry on powder performance as well as explore inter-relationships among powder characteristics.

Surface Area

The effects of powder granulometry on oxide contamination could be evaluated based on the particle size and amount of coarse and fine particle composition found in various powder grades. In other words, multimodal or skewed powders may tend to contain higher concentration of fine particles and exhibit larger net surface area as compared to *Gaussian* distributed grades. Also assuming that majority of the powder particles are highly spherical with uniformly distributed interstitial films encapsulating such particles, the specific surface ($\frac{\mathrm{A}}{\mathrm{V}}$) can be simply derived using the sphere formula $(\text{Surface Area, } \mathrm{A} = 4\pi r^2)$ and $(\text{Volume, } \mathrm{V} = \frac{4}{3}\pi r^3)$ where the radius, r represents the mean particle size. Technically, the degree of contamination should increase with reducing mean powder size due to surface area enlargement [132]. This is shown in Figure 25 where an increase in specific surface with decreasing particle size (D90) was observed for different metallic powders used in SLM. In this context, oxidation could occur more rapidly in fine powders having higher specific surface values as compared to coarser sized grades.

Another method used to measure powder surface area refers to the Brunauer, Emmett and Teller (BET) analysis which determine the amount of physical adsorption on particle surfaces via the displacement of adsorbate gas allowing the total surface area of a powder mass to be evaluated [16]. In Simchi's study [133], the BET technique was used to compare the surface area of GA and WA iron powders of various mean particle sizes used for direct metal laser sintering (DMLS) where powder A (MPS = 13.4μm) which contained the smallest particles was observed to possess the highest surface area (S_a = $4202 m^2/g$) among the powder grades as shown in Table 2. The amount of oxygen content found in the GA powder was fairly high (O = 0.12%), which was unusual given its atomisation nature. The oxide content in GA powder could suggest an increase in surface area caused by the refinement of particle size, leading to higher oxygen inclusions. Additionally, the highest oxygen content found in powder B could highlight compounded effects of high oxide inclusions due to WA and reducing mean particle size. Meanwhile, previous studies [71,133] had highlighted that the enlargement of surface area following the use of finer sized particles was particularly favourable to part densification by increasing laser absorption. However, the risks of powder contamination may also increase which lead to processing issues (E.g. Balling) and is expected to be more pronounced when synthesizing highly reactive alloys. Oxide films surrounding powder particles also exhibit melting points much higher than the parent metal which are difficult to break down without the aid of higher energy density levels. Even if successfully melted, some of the undissolved oxide compounds could substantially raise laser absorptivity [124] and increase melt pool temperature, possibly creating larger gradients that may further lead to higher residual stresses accumulated in the solidified part. However, more studies are required to perform surface area analysis for AM feedstock in order to establish a conclusive

relationship between different size distribution models and surface area data as well as correlate with oxygen content measured to quantify the effects on powder contamination.

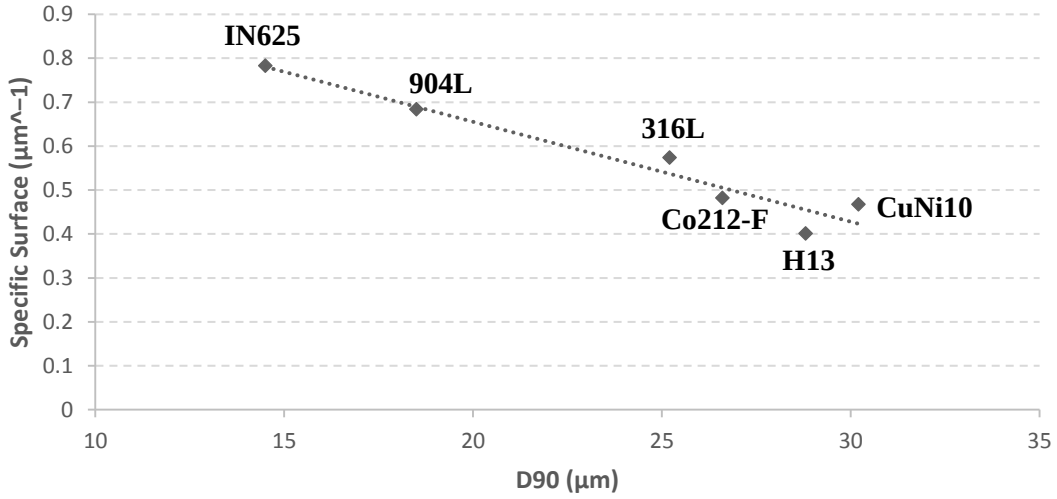

Figure 25: Powder size (D90) vs Specific surface [117]

Table 2: Characteristics of Fe powders [133]

Powder	Atomization Type	Oxygen Content (%)	Mean Particle Size (µm)	Surface area (m^2/g)
A	Gas	0.12	13.4	4202
B	Water	0.59	29.2	2670
C	Water	0.11	42.6	2819
D	Water	0.07	51.3	2886
E	Water	0.07	69.4	2190
F	Water	0.07	106.4	1143
G	Water	0.07	174.5	1976

Packing Density

Generally, powder grades with a wide size distribution and adequate amounts of fine particles present in its distribution array will tend to exhibit high packing densities. In powder metallurgy, powder size distribution was believed to pose the greatest influence among other characteristics on the packing behaviour of powdered materials [134]. A few empirical models were also developed in the past to study powder packing configurations relative to particle size distribution [135–138]. The studies illustrated different methodologies used to optimise powder packing density for two main types of size distributions: (1) Continuous (*Gaussian*) and (2) Discontinuous (Multimodal). A fundamental concept was shared across the studies where packing efficiency was mainly improved through the reduction of

void interstices in a coarse powder matrix by adding finer sized particles comparable to the pores found in the loose granular network. The Andersen's Equation focused on improving the powder packing density of *Gaussian* size distributions by incorporating fine particles of infinite size to fill up random vacancies among coarser particles [138]. However, the numerical approach may not be feasible for SLM powders since particles below 10µm will have to be used, thus creating powder handling issues. Nevertheless, it was proven that powders with a wide size distribution exhibited better packing behaviour over narrow size distributed ones where the inclusion of fine particles extended the size distribution width with predicted optimal packing densities peaking at 96% [139]. Additionally, a widened size distribution also increases its standard deviation which has shown to decrease void sizes and reduced the overall packing porosity [140]. For powders used in SLM processing, a similar granulometry influence on packing density could be observed where Liu et al. [85] reported that powders having a skewed size distribution (Osprey) contained higher amount of fine particles (0 - 45µm) (as shown in Figure 26) also exhibited higher apparent, powder bed and tapped densities of more than 4% as compared to a typical *Gaussian* distributed grade (10 - 45µm). The tapped densities of Ni alloy powders reported in Engeli et al.'s study [78] were also higher with increasing size distribution spans (Refer to Figure 27). The difference in density values was however, less significant among powders with comparable span values while saturation of tapped densities may be observed in powders with distribution spans ≥1.5.

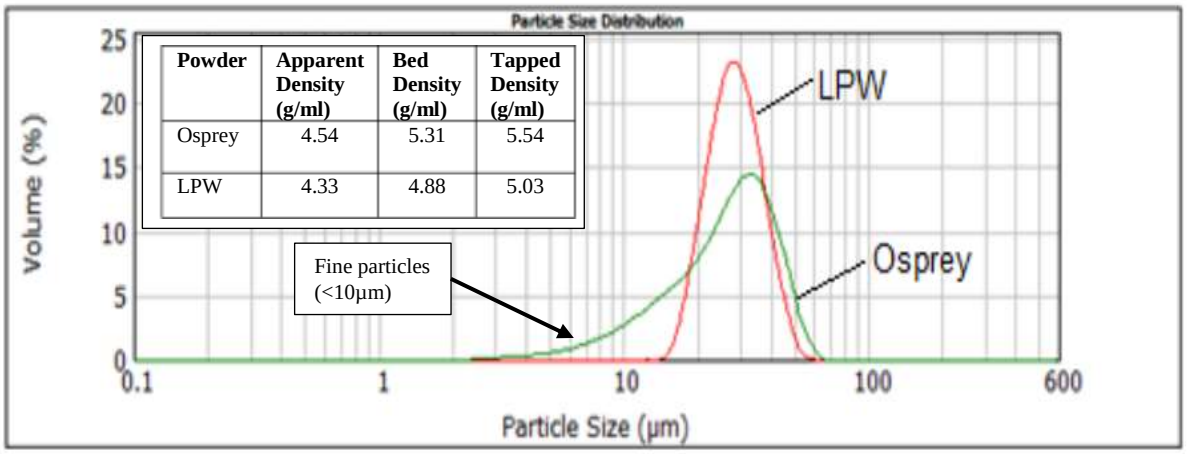

Figure 26: Powder characteristics of LPW and SO powder [85]

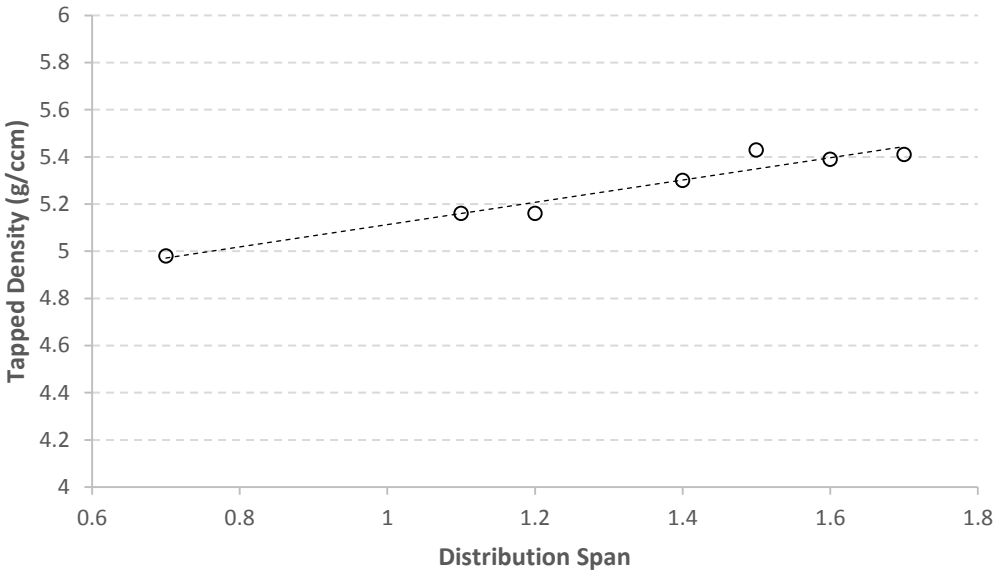

Figure 27: Powder Distribution Span Vs Tapped Density [78]

The Furnas Model [136] is another approach used to enhance powder packing density through adding fine particles of discrete diameters and effectively percolate through known void sizes in a coarse powder matrix, generating a multimodal size distribution with secondary or tertiary peaks. As shown theoretically, the packing density of mono-sized powder in an orthorhombic arrangement can be increased from 74% to 84% (Refer to Table 3) following the addition of fine particles equivalent to the size of its inter-particle voids [141]. A third component addition can also further expend the remaining voids to reach a higher packing density of 95.7% [142]. Although actual powders hardly arrange in an ideal manner, the same packing densification technique can be employed through the combination of coarse and fine powder grades with narrow size distributions to achieve an optimum composition and size ratio which exhibits maximum packing density (Refer to Figure 28). The size ratio between coarse and fine particles is also usually determined based on the existing void size and morphology of the base powder while the quantity of fine particles to be added depends on the apparent densities of the respective powders. It was also shown earlier that effective packing density improvement commences at a coarse to fine size ratio of 1:7 where fine particles were able to percolate through triangular pores in the coarse matrix [141]. 30% of fine powder was added to the coarse base and the maximum achievable packing density was 84%. The bimodal approach was later adopted by [69] to improve the packing density of DMLS Ni powders. Using a size ratio of 10:1, powder layer density was reported to increase from 53% to >60% following the addition of 30% fine particles. Zhu et al. [142] also reported that the apparent density of Cu alloy powder was enhanced from 76.9% to 87.6% when the amount of fine binder particles increased by 10%. Olakanmi et al. [105] studied multimodal blends of Al powder where a tri-modal grade containing coarse, medium and fine particles with size ratio of 5:2:1 and 75:20:5wt% composition ratio showed a slight increase in tapped density (~3%) over bimodal grades following the inclusion of fine particles (10 - 14µm). Based on the literature, addition of fine particles was found to be influential in modifying powder packing density which could either skew a *Gaussian* distribution or generate a multimodal distribution wherein both approaches result in the extension of size distribution widths. Additionally, the multimodal approach may offer a more straightforward solution to improve packing behaviour as void sizes are typically predetermined as compared to a random distribution of unknown voids. However, it is challenging to define a standard size distribution which provides the optimum packing behaviour despite existing methods shown to enhance powder packing density through fine particles inclusion since powder flowability will also be concurrently affected which will be discussed in the next sub-section.

Table 3: Packing arrangement and density of different distribution models [142]

Type of Distribution Model	Unimodal	Bi-modal	Tri-modal
Particle packing arrangement	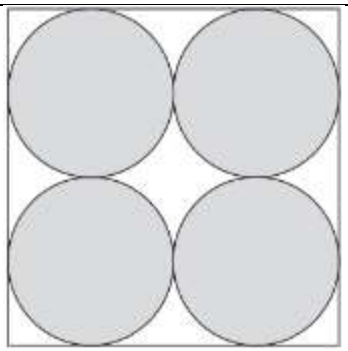	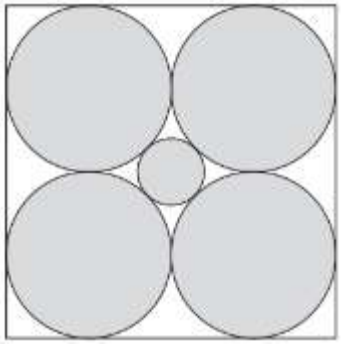	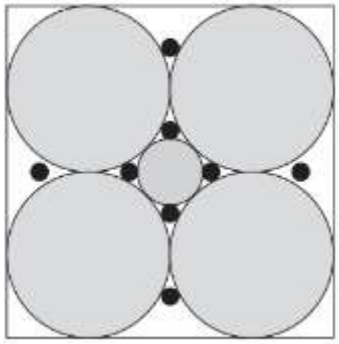
Packing Density Achievable	74%	84%	95.7%

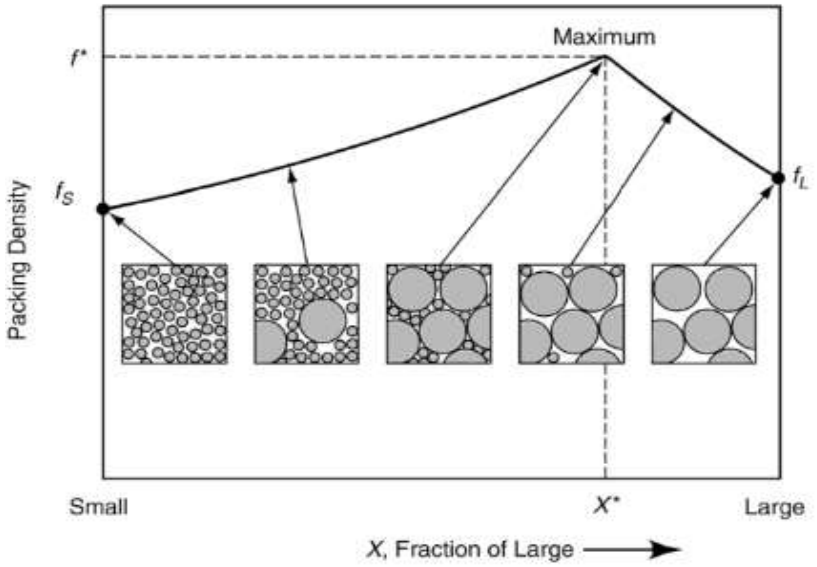

Figure 28: Particle size composition vs Packing density [143]

Flowability

As the aforementioned, blending of fine particles with coarse powder can provide beneficial effects towards improving powder packing density through effective size mixing and percolation. However, the incorporation of fine particles, on the other hand, could introduce certain drawbacks on flowability due to increased powder cohesion and inter-particle forces. Particle adhesion forces including *Van der Waals* attraction is typically more inherent to fine particles where agglomeration starts to form easily, increasing inter-particle friction which constitutes to poor rheological behaviour. Powder particles below the size of 30μm would also more likely experience agglomeration problems, as shown in [133] where the agglomeration factor (φ = Powder bed density/tapped density) was less than 1 ($\varphi \approx 0.80$) in iron carbonyl powder grades with mean particle sizes <30μm which indicated the presence of agglomeration. As illustrated in Figure 29, powder flowability becomes more restricted with decreasing particle size [54]. The resulting agglomeration effects could also be detrimental to powder apparent density since fine particles would mostly adhere with each other, forming irregularly shaped powder clusters instead of filling up the inter-particle voids within the coarse matrix.

By comparing the flow behaviours of different powder size distributions, wider size distributed grade would experience flow degradation over a narrower grade with HR of 1.22 and 1.16 respectively as shown in Figure 26. While both powders were still considered free-flowing, a wider size distribution width may have led to a reduced rheological performance as reflected on the ~5% decrease in HR. Similar observations were found in Engeli et al.'s work [78] where powders with larger size distribution spans induced reductions in flowability. Figure 30 was replotted from the study which showed powder distribution spans ≤1.5 exhibited good flow ($HR \leq 1.25$) while spans >1.5 displayed signs of flow resistance ($HR \approx 1.26$-1.32). In particular, most powders with distribution spans above 1.5 (except Powder D) contained at least 15% of particles that were smaller than 10µm which may emphasize on the reduced flowability effects due to fine particles presence. In another study by Gu et al. [103], a bimodal Ti6Al4V powder containing higher amount of fine particles exhibited higher flow resistance (AOR = 55.2º) as compared to *Gaussian* grades (AOR = 40.1º and 31.8º) measured using AOR method. The wider distributed *Gaussian* powder with larger standard deviation (SD=10.18µm) behaved more cohesively than the narrower grade (SD=8.71µm) which could reiterate on the influence of distribution widths on rheological behaviour. Despite having an intermediate standard deviation (SD=9.7µm), the bimodal grade displayed the least flowability which could further suggest a more detrimental influence on powder rheology when containing excessive amount of fine particles (Multimodal) as compared to increasing powder spans (*Gaussian*). Hence, the addition of fine particles should be proportionated between achieving maximum packing density and flowability to optimise powder performance. Additionally, other factors which result in flow deterioration should also be considered including surface area enlargement due to particle size refinement, irregular particle morphology and poor surface conditions (E.g. moisture, rough oxide skins). It would also be a huge challenge for the SLM process if further process layer thickness reductions were to be made for achieving better part precision, since particles finer than (D_{10}<10µm) may be required to generate suitable powder layer densities based on Karapatis et al.'s size criteria [69].

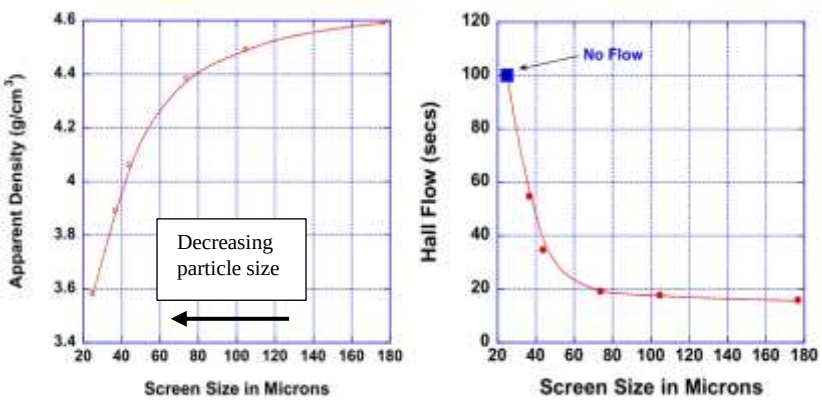

Figure 29: Powder size vs Apparent Density (left) and Hall Flow (right) [54]

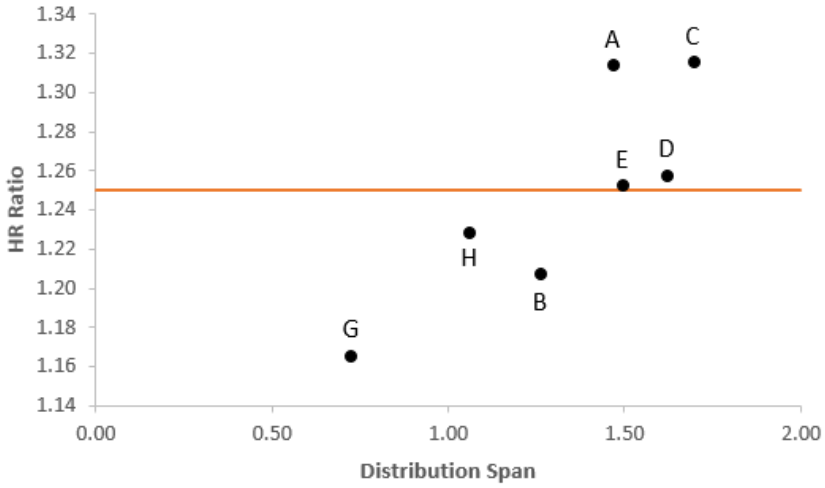

Figure 30: Distribution Span vs Hausner Ratio (Redrawn from [78]*)*

Thermal Properties

Relative to powder granulometry, the resulting packing density and local particle arrangement under the laser beam would greatly affect thermal interaction between the irradiated source and deposited feedstock. In other words, the degree of laser absorption varies with the number of particles exposed under the irradiated beam area where higher thermal absorptivity is achieved when powder packing density increases, involving greater surface reflections within a closely packed cluster of particles. Using the ray tracing model, Boley et al. [124] observed higher average laser absorptivity in a bimodal powder grade with size ratio 7:1 and 20% fine particles content as compared to a *Gaussian* distributed powder with mean particle size of 27µm (refer to Figure 31). The higher concentration of fine powder in the bimodal configuration increased the number of particles' presence under beam coverage which was associated with the higher probability of particle surfaces being irradiated, thus increasing laser absorption. In a separate study, the increase in laser energy absorption could also be due to the refinement of powder mean particle size which allowed the enlargement of powder surface area exposed to the irradiation source according to [133]. However, thermal absorptivity values often fluctuate over different points along the powder bed due to the arbitrary dispersion behaviour of actual powders which constitutes to variations in local particle packing exposed to the laser source. In addition to thermal absorption pattern analysis, OPD could help to further understand the effects of powder granulometry on thermal interaction, where the amount of unabsorbed irradiation energy which is reflected off powder surfaces and transmitted further into underlying particles and/or substrate through multiple scattering can be evaluated. Earlier, Fischer et al. [29] observed a ten-fold difference in OPD (20µm vs 200µm) between Ni powder grades with particle sizes <20µm and 50-75µm respectively. Since the depth of beam infiltration associated with OPD is dependent on the packing density and size distribution, a powder bed with high packing density would generally allow lesser irradiation beam to permeate through which then exhibit a smaller OPD with increased thermal absorptivity as compared to a porous configuration. Zhang et al. [22] also reported that the melting of fine Fe powder (<20µm) obtained a higher solidified melt track height as compared to a coarser sized powder (20µm< d <42µm). The higher apparent density of the finer sized powder reduced laser transmissivity (low OPD) and achieved greater melt pool volume as compared to the coarser grade. OPD also provided a measure of process layer thickness required where fine particle sizes with high packing densities generally require thinner layers to generate a sufficient melt pool volume [118]. Based on the reported studies, it could suggest that powders with high packing density would allow more irradiated source to be absorbed effectively at the deposited layer and minimise beam transmission reaching the underlying substrate.

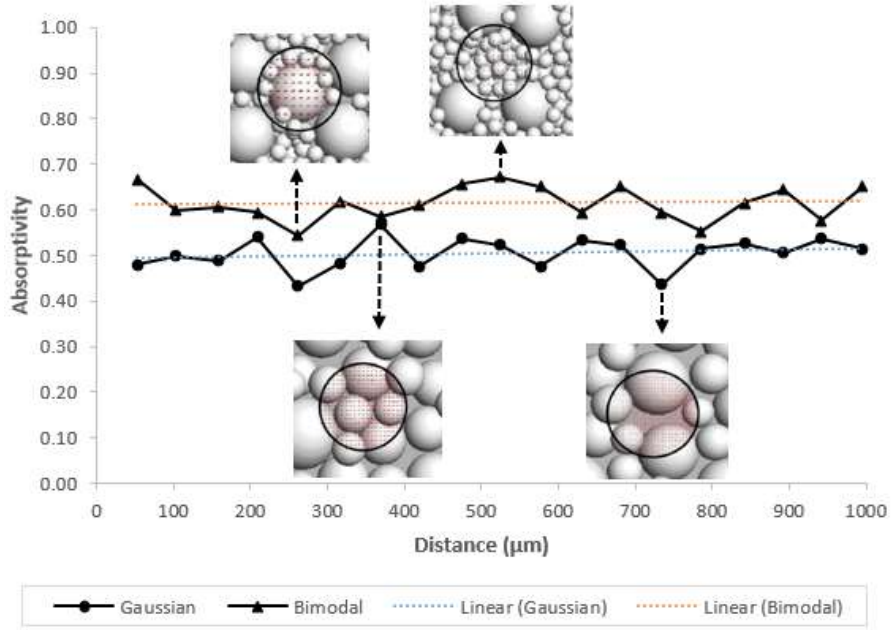

Figure 31: Thermal absorptivity Comparison between Bimodal and Gaussian powder [124]

Powder particles are typically arranged at point contacts with each other within a powder bed while the inter-particle gaps are often filled with the inert atmospheric medium which are poor conductors of heat. Hence, the ability for a powder bed to effectively conduct heat away from the melt pool and through the surrounding particles during the SLM process is mainly dependent on the packing configuration under the influence of its size distribution instead of the bulk thermal conductivity of material. It was shown in [144] that a higher relative packing density increases the thermal conductivity of metallic powders (refer to Figure 32). Accordingly, high coordination number and increased powder particle contacts can also correspond to a larger degree of heat transfer. This was demonstrated by Gusarov et al. [145] where mono-sized spheres with the densest packing configuration (FCC) and highest coordination number (N = 12), obtained the highest thermal conductivity as compared to other crystal structures (BCC, SC and Diamond). Particle packing models were also simulated by Zhou et al. [146] whom reported that a bi-modal powder configuration exhibited two distinct coordination numbers which corresponded to the individual particle contacts of coarse and fine powder respectively (Refer to Figure 33). The bimodal mixture consisted of fine particles with a lower coordination number (N = 4) and coarser particles (N = 8) while a mono-sized powder displayed only a single coordination number (N = 6). Despite this discontinuous trend of particle contacts observed in multimodal powders, the thermal conductivity of bi-modal Ti6Al4V powder was still 40% higher than the *Gaussian* powder grades as reported by Gu et al. [103]. With respect to earlier studies, the inclusion of fine particles in the bi-modal powder could provide better packing performance, but its effectiveness on improving thermal conductivity due to increased packing density or higher coordination number/particle contacts remains unclear, requiring more detailed thermal conductivity measurements of powder grades with different granulometry data. Such thermal conductivity values would be useful for future laser-powder bed numerical simulations and heat transfer models in achieving better powder to part quality predictions.

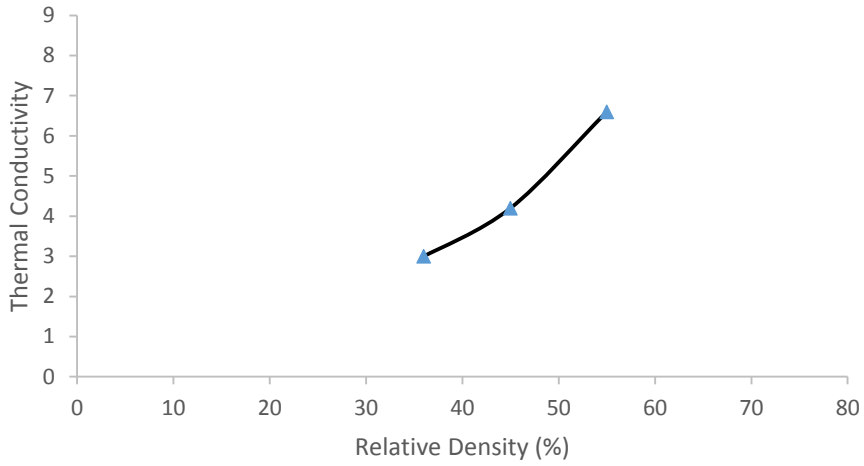

Figure 32: Relative powder density vs Thermal Conductivity Ratio [144]

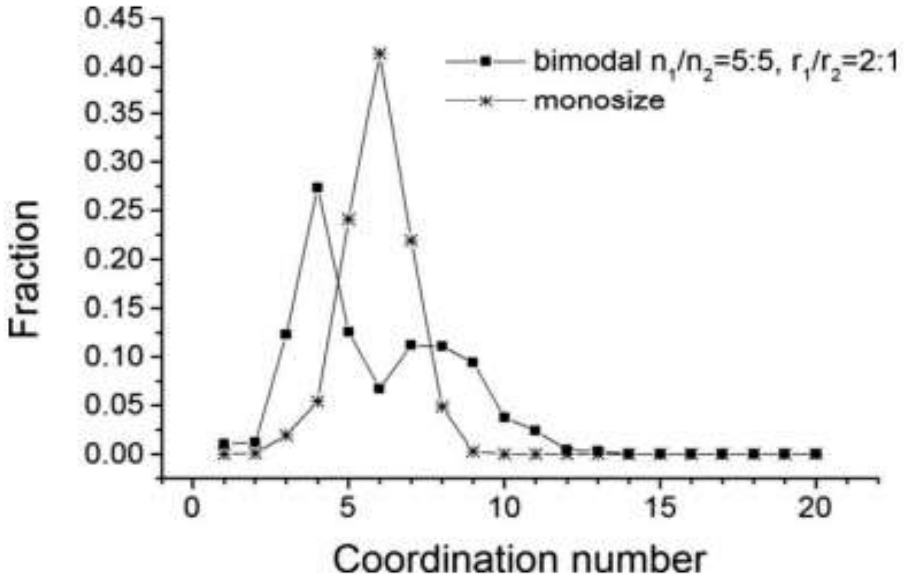

Figure 33: Particle fraction vs Coordination number [146]

5.2 Effects of Powder Granulometry on Part Performance

The potential influence of powder granulometry on the various part characteristics including density, mechanical properties, microstructure and surface quality will be discussed in the following sections.

Part Density

Part density is a primary quality metric which determines the usability of components manufactured via additive means including SLM. Apart from applications which require porous materials, SLM components are otherwise preferred to achieve high part density (>95%) as residual porosity often result in the degradation of mechanical properties and overall part performance [147]. Porosity defects are commonly found in SLM parts as consequences of powder related faults and unsuitable processing parameters used which lead to shrinkage, balling and vaporisation effects [9]. Additionally, secondary powder characteristics such as high oxide content in chemical composition and poor packing density are known to cause adverse effects on part densification. However, the primary influence of powder granulometry on final part densities was less discussed in the literature but could present potential effects of part densification related to size distribution.

Spierings et al. [58] reported that part density produced by 316L powders with different size attributes was strongly tied to the process windows used. A *Gaussian* grade with the finest granulometry (D_{90}=30.8µm) obtained the best part densities across all energy density levels and layer thicknesses (30µm and 45µm) used. Presence of fine particles (<10-15µm) in the coarsest negatively skewed powder (D_{90}=59.7µm) also generated better part densities than an intermediately sized *Gaussian* grade (D_{90}=41.3µm) at layer thickness of 30µm and low energy density range of 35 – 60J/mm^3. However, the increase in layer thickness to 45µm showed that the finer sized powder produced denser parts since more complete melting was achieved as compared to the coarser skewed grade. Accordingly, the higher concentration of fine particles in the skewed powder facilitated more pronounced melting at 30µm layer while the effect was later diminished at 45µm layers (effective layer thickness = ~74µm) where preferential melting occurred, based on the overall powder size. Essentially, the use of powders with fine granulometry could provide better densification of parts than coarse grades by means of achieving the complete melting of particles. Liu et al. [85] compared 316L grades with different distribution widths and reported better part densification results in the wider distributed powder (SO) at scan rates >150mm/s while the narrower grade (LPW) performed better at a slower scan speed (100mm/s) (Refer to Figure 34). It could suggest the higher tendency for finer particles to vaporise at low speed and high energy density conditions which likely initiated keyhole melting and induced porosity upon solidification. In addition, coarse powder grades may be less affected with increasing energy density since larger particles would require longer periods to achieve complete melting which reduced the probability of material vaporisation. As the scan speed was raised to 150mm/s and above, the SO powder generated higher density parts than LPW which could suggest the beneficial effects of fine particles in promoting rapid melting without vaporisation occurrence. Gu et al. [103] compared the part densification effects between *Gaussian* and multimodal Ti6Al4V grades which revealed higher porosity in *Gaussian* Ti6Al4V powders over a bimodal grade. The higher thermal conductivity of bimodal grades was said to generate a wider melt pool which permitted more melt overlaps, thus preventing the formation of pores between adjacent tracks. Besides, the more efficient powder packing behaviour of multimodal powders could have contributed to higher part densification according to [105]. Based on these studies, the usage of fine granulometry powders would generally require lower energy densities to achieve the complete melting of particles as compared to coarser grades. Moreover, the inclusion of fine particles aid in part densification associated with powder packing density enhancement but requires complementation with process parameters in order to achieve optimum results. Meanwhile, further studies are required to validate the size and composition of fine particles allowable before powder vaporisation occurs which could draw relations to the packing density as well as thermal absorptivity of the powder.

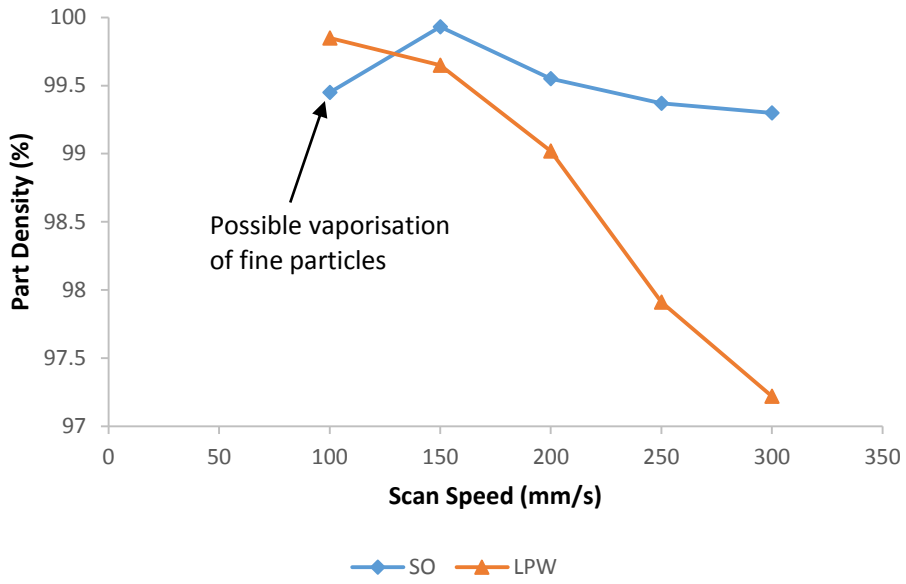

Figure 34: Part Density of commercial 316L powder at different scan speeds [85]

Mechanical Properties

A key initiative of metal additive manufacturing adoption is to produce structural components with superior performance as compared to traditional machining or casting methods. The mechanical properties of metal AM components are therefore expected to be equivalent if not, surpassing parts fabricated by conventional techniques in addition to design flexibility and material efficiency benefits. In essence, SLM parts are often produced with high tensile strength and better hardness but present lower ductility and decreased fatigue performance as compared to wrought products [148–150]. Anisotropic behaviour also exists in SLM parts where part mechanical properties are dependent on the build orientation, scan strategy as well as part layout [151–153]. The influence of process variables on mechanical properties including laser power, scan speed, layer thickness and hatch spacing were also extensively studied and well documented in the literature [154–156]. With regards to powder characteristics, oxide and other non-metallic inclusions in the material composition are known to segregate at molten pool boundaries which solidify as grain boundaries and affect the mechanical properties [152]. However, the influence of powder granulometry on mechanical properties is not well understood and may have potential contributions related to part porosity.

Spierings et al. [79] reported that a coarser granulometry powder could contribute to larger void sizes in fabricated parts as compared to finer powder grades. Despite exhibiting a negatively skewed feature (presence of fine particles), the coarsest powder grade produced parts with relatively lower mechanical strength in which there could be insufficient amount of fine particles to effectively fill up large voids among the coarse powder matrix. The enlarged pore sizes act as crack initiators during tensile loading and result in lower ultimate tensile strength (UTS) of SLM 316L parts produced by coarser grades. On the other hand, fine granulometry showed lower ductility which could be due to higher laser absorption under a larger surface area which extended the degree of undercooling, leading to a finer microstructure and higher tensile strength. In another work, Liu et al. [85] used two different 316L grades with comparable mean sizes where the wider size distributed powder (negatively skewed) produced parts with lower strength and higher elongation as compared to the narrower grade. In contrast to Spierings et al. [79], the presence of fine particles may have induced quicker melting and prolong melt pool life, producing coarser grain structures which reduced mechanical strength. Meanwhile, parts produced by bimodal Ti64V powder showed slightly higher UTS and lower yield strength over *Gaussian* grades as reported by Gu et al. [103]. Due to contradictory reports, more experimental validation studies and

microstructural evaluation are required to quantify the degree of powder granulometry influence on mechanical properties particularly on the size and composition of fine particles to be used.

Microstructure

Metallic components fabricated via the SLM process often display microscopic characteristics different from traditional casting techniques in terms of grain size, growth morphology and phase formation due to the rapid heating and freezing cycles [157]. The extreme cooling rates (10^3 to 10^8 K/s) typically yield relatively finer grains (<1µm) as compared to conventional solidification methods and may also allow the nucleation of metastable phases which deviates from equilibrium conditions. Growth patterns of solidifying grains depend strongly on thermal gradients of the melt pool where planar solidification usually takes place at the interface between melt pool and substrate before evolving to cellular and dendritic structures. Under narrow solidification windows, the diffusion process is often limited which rarely allow the occurrence of second phase precipitation or structure segregation while refined primary and secondary grain features are typically obtained, providing remarkable mechanical strength for SLM parts [13]. Grain sizes in SLM parts are also controllable through the modification of process settings where faster scan speeds and lower resulting energy densities were shown to produce finer microstructures [28,45]. The increase in scan velocity was said to provide a larger degree of undercooling at the melt pool which resulted in quicker solidification rates and grain growth inhibition.

In terms of feedstock influence on part microstructure, chemical composition of starting powders were reported to affect the formation of micro-constituent phases [3,82]. It was shown by Starr et al. [82] that parts manufactured using 17-4 PH SS powder produced via nitrogen gas atomisation contained a mostly austenite structure (>96%) while an argon atomised powder achieved a more martensitic structure (~76%) even though both powders were processed under the same SLM environment. The higher content of residual nitrogen in the starting powder was believed to enable austenite retention and stabilised the FCC phase instead of transforming to martensitic structures. On the other hand, increasing oxygen concentrations were reported to reduce grain sizes in Fe parts by Simchi [133]. Due to the presence of oxide films, it could have increased the amount of laser absorption and induced a steeper thermal gradient which generates a larger degree of undercooling for more rapid solidification to occur. Since process cooling rates have strong affinity to the thermal interaction between laser and powder, thermal properties relative to its packing density as well as powder granulometry could also impose some influence on part microstructure. Averyanova et al. [158] compared the microstructure of PH 17-4 parts produced from two GA *Gaussian* powders with different powder sizes (D_{90}<16µm and D_{90}<25µm) where the finer powder generated higher concentrations of martensitic phase (38%) as compared to the coarser grade (6%). Another study by Olakanmi et al. [105], reported that the bimodal Al-Si powder which exhibited the highest tapped density, also achieved the most refined dendritic feature among other bimodal blends. Both studies could suggest that fine particles may allow higher heat conduction away from the melt pool and faster quenching ability associated with the finer microstructure results. However, more refined particle sizes (<14µm) found in tri-modal Al-Si blends could induce extended melt pool life which facilitates grain growth as compared to bimodal powders (<30µm). Nevertheless, further investigations are required as other powder variation studies showed limited evidence on microstructural changes including [103] whom reported similar grain growth and constituent phases across bimodal and *Gaussian* Ti6Al4V powders. Ardila et al. [65] also observed comparable growth behaviour of columnar grains with dendritic structures aligned to the build direction (Z-axis) in new and recycled IN718 powder batches despite a difference in granulometry. By comparing the type of materials used in the mentioned studies [65,103,105], subtle changes in cooling rates which affect the microstructure could be more observable in better conductivity materials (Al alloy) as compared to other materials (Ti and Ni alloys). Overall, the primary influence of granulometry on microstructural changes is still limited with no direct correlations although possible links between powder thermal properties and the resulting microstructural size could be realised with regards to the

variation of powder size distribution and packing density that affects heat transfer rates during the SLM process.

Surface Quality

Surface roughness is an essential indicator which determines the build quality of AM components especially for cyclic applications that require excellent surface quality (Ra = ~0.8μm) in order to prevent premature fatigue failures [159]. While the average surface roughness of as-built SLM parts (Ra = 8.75 μm) [4] is typically better than other metal AM techniques, it is still an underlying challenge to achieve machine-finished surface quality without additional operations such as polishing, shot peening or abrasion. In-situ, the Laser surface re-melting (LSR) technique is used to refine rough contours at the periphery layers through the redistribution of melt pool to evenly fill up voids and improve surface quality (Ra=1.5 μm) [109]. However, the re-melting strategy remains a costly and time-consuming procedure since every layer must be re-scanned to produce highly dense and surface enhanced parts. Most AM built structures also exhibit a stair-step appearance due to the layer-by-layer forming nature which approximates contours of produced components especially for features built at low sloping angles (5-15º) from the substrate. Meanwhile, steeper profiles (>20º) minimise gaps between stair-step intervals but contribute to surface roughness by increasing the number of partially melted particles residing at slanted edges [160]. In addition, the top surface roughness (perpendicular to build direction) is mainly created by rippling motions of the melt pool while side surface roughness (parallel to the build direction) is the likely outcome of segregated melt drawn to the layer edges under Marangoni convection and surface tension effects [161]. Subsequently, geometrical characteristics of the solidifying melt pool would play a strong role in determining the surface roughness of each finished layer during part build-up. In fact, the most common surface defect also known as balling phenomenon is a result of melt pool breakages under high scanning speeds which generate discontinuous surfaces that obstruct coater movement and initiate porosity through non-uniform powder deposition [13,40]. Surface quality degradation due to balling is also more prevalent at the side roughness following the residing motion of the melt pool. On the other hand, large melt pools produced by low scan velocities and/or high laser power could also generate rough layer surfaces upon solidification and induce balling [162]. Adequate laser energy input should be used to flatten the melt pool under recoil pressure and obtain smoother surfaces [29,161]. Layer thickness reductions can also minimise the stair-stepping effect by reducing stair widths but usually demand longer build times as more number of layers needs to be formed [160,163,164]. Narrower hatch distances also improve surface roughness of parts which facilitate melt overlaps between adjacent tracks [26,162]. Most of these effects were related to the energy density used in the SLM process where researchers have developed various physical and numerical models to predict surface quality [160,165,166].

With regards to powder characteristics, part surface quality is directly affected by powder granulometry where the use of finer particles can minimise stair-stepping effects since smaller layer thicknesses are required [79,167]. Correspondingly, the use of refined powder sizes and layer thicknesses allows SLM to outperform other metal AM systems in terms of surface quality and part resolution [9]. Powders with fine granulometry would also be more substantially melted and generate better surface quality over coarser grades as shown by Spierings et al. [79]. Furthermore, a wider distributed powder (0-45μm) produced parts with better side surface roughness as compared to a narrower grade (10-45μm) [85]. Using numerical simulations, Lee and Zhang [100] also presented that a positively skewed powder with higher composition of fine particles generated a smoother melt pool surface as compared to a negatively skewed grade of similar particle size range. However, fine powders may impose a disadvantage when building sharp edges with an inclination (~45º) due to heat accumulation effects, producing rougher surfaces [167]. Based on the reported studies, the surface quality of SLM parts seemed to be mainly affected by powder granulometry in terms of layer thickness and powder packing density. Powders with fine granulometry would generally require smaller layer thicknesses which could reduce the stair-stepping effect as well as surface roughness. On the other hand, the inclusion of fine particles which

concurrently increase powder packing density would also generate a stable and continuous melt pool, producing smoother contours and part surfaces.

6.0 Summary

The influence of powder granulometry on feedstock and part performance in the SLM process has been reviewed in this work and summarised in Tables 4 and 5 respectively. Powdered materials used in the PBF technique often vary in size distribution due to process disturbances (mechanical, thermal etc.) which extends over other powder characteristics as well as affecting final part quality. As such, it is important to survey the various processing implications due to granulometry changes and establish further grounds for feedstock manufacturing, optimisation, characterisation, qualification as well as selection specially tailored for the SLM process. Among powder characteristics, morphology and granulometry attributes are primarily intertwined which can dictate other physical and chemical behaviours of the feedstock. Packing density and flowability form the basis of feedstock qualification prior to SLM processing and are directly affected by granulometry variations which demand strong emphasis for optimization of the respective parameters.

Higher powder packing density is typically observed in wider *Gaussian* distributed grades with skewed features and multimodal powder distributions where small proportions of fine particles are intentionally added to percolate through packing voids among coarse powders under a suitable size and composition ratio. In comparison, more significant powder packing density improvements may be noted for multimodal powders (≥10%) over skewed *Gaussian* grades (<5%). Accordingly, enhancements in powder packing behaviour can increase particles' presence under laser exposure which raise thermal absorptivity during consolidation, both corresponding to higher part densification. In addition, improved packing also allows the increase in powder bed thermal conductivity, involving more number of particle contacts for enhanced heat transfer. However, fine particles (<10µm) added in excessive amounts (>15%) would tend to reduce powder flowability and affect coater performance during deposition, resulting in possible segregation or agglomeration. Based on the inverse relationship between powder packing density and flowability, multimodal powders are also more likely to encounter flowability issues as compared to *Gaussian* grades.

In terms of overall particles' size, fine granulometry will generally expose a larger surface area during laser irradiation which facilitates complete melting to produce dense parts. However, there may be increased risks of powder contamination as compared to coarser powders. Meanwhile, coarse granulometry introduces larger void sizes which act as crack initiation sites in produced parts and reduces mechanical strength. The relatively higher laser absorptivity of fine particles would also increase the undercooling degree which enhance solidification rates and produce more refined microstructural features. This could also explain the lower elongation observed in finer powder grades. Subsequently, steeper thermal gradients can yield greater percentage of metastable phases but may contribute towards higher induced residual stresses. The influence of granulometry on surface quality is also clear where finer powders generate smoother part surfaces as smaller process layer thicknesses are needed. To further evaluate granulometry influence on part properties, it is necessary to derive appropriate process parameters used to comply with powders of different granulometry characteristics.

Current Best Practices and Challenges

Based on the analysis of feedstock used in SLM and DMLS processing, basic powder requirements that are currently in place to ensure good process-ability are designed with the following conditions:

- D_{90} of the feedstock should be smaller than the process layer thickness used ($D_{90} < t_{layer}$) in order to prevent the segregation of particles with sizes larger than the allocated thickness

- Feedstock used should possess uniform sphericity and apparent density as high as possible while maintaining good flow behaviour to promote densification and minimise agglomeration effects concurrently
- Metallic feedstock should contain very low levels of interstitial contaminants such as oxygen and hydrogen due to their adverse effects on SLM processing in disrupting layer adhesion and disrupting part properties

Current industry SLM applications still mainly utilise *Gaussian* powders which may be due to the tedious pre-requisite preparation involved during feedstock mixing and blending procedures to produce skewed or multimodal feedstocks. Furthermore, there are insufficient studies which evaluated on the performance of AM feedstocks affected by granulometry variations (*Gaussian*, positively/negatively skewed, bimodal, trimodal etc.) to explicitly study the powder behaviour (density, flow etc.) and influence on finished parts. The inverse relationship between powder packing density and flowability also further complicates the decision to integrate fine powders which demands extensive experimental trials to identify powder formulations of appropriate size and composition ratios of coarse and fine particles tailored for SLM. Current flow and density criterions used for the characterisation of AM powders are also mostly adapted from existing test standards designed for traditional PM which may not be directly transferrable to laser processing techniques which involve rapid melting and re-solidification mechanisms. As compared to thermal particulate diffusion studies in conventional sintering, the focus for SLM processing should be emphasized on the thermal history of powders with different granulometry that could possibly yield various molten pool structures (volume, geometry, morphology, wetting behaviour, surface tension etc.) and affect formed layers with consideration of Marangoni convection and vapour pressure above the melt surface. Till now, melt formation during SLM processing under granulometry influence is still not well understood and difficult to characterise but is believed to involve the combined effects of various feedstock parameters including packing density, flowability, surface area and thermal absorptivity related to its size distribution.

Table 4: Effects of Powder Granulometry on Powder Performance

Powder Characteristic	Key Findings	Reference
Surface Area	• Fine powders exhibited larger surface area as compared to coarse powders, providing higher amount of laser absorption	[105]
Packing Density	• Higher powder bed density was observed in 316L powder with wider size distribution	[75]
	• Powder layer density increased from 53% to 63% via the addition of 30% fine particles and size ratio (1:10) in Ni-based powders	[50]
	• Increase in tapped density observed in IN738LC powders with increasing size distribution spans	[53]
	• Increase in apparent density from 76.9% to 87.6% for Cu alloy powders when the amount of fine binder particles (<20μm) increased by 10%	[113]

	• Highest apparent and tapping densities observed in trimodal blended Al-Si powder of coarse-medium-fine size ratio 5:2:1 and composition ratio 75:20:5wt% respectively	[73]
Flowability	• Mean particle size smaller than 30µm tend to agglomerate easily	[105]
	• 316L powder with narrower size distribution exhibited better flowability	[75]
	• Reduction in flow energy from 665mJ to 658mJ observed in recycled titanium powder as compared to new powder	[45]
	• Poorer flowability observed in bimodal Ti6Al4V powder with higher AOR of 55.2º as compared to *Gaussian* grades	[74]
	• IN738LC powders with distribution span ≤1.5 (HR≤1.25) exhibited better flow than those with spans >1.5 (HR≈1.26-1.32)	[53]
Thermal Properties	• Simulated bimodal powder with size ratio 7:1 and 20% fine particles inclusion showed increase in absorptivity over *Gaussian* grade	[96]
	• Lower OPD (20µm) observed in fine particle sizes (<20µm) as compared to coarse Ni grade (50-75µm) with OPD of 200µm	[89]
	• Melting of fine Fe powder (<20µm) as compared to (<45µm) produced more melt volume due to lower OPD and higher energy absorption which formed larger track heights	[16]
	• Thermal conductivity of bimodal Ti6Al4V powder was 40% higher than *Gaussian* grades	[74]
	• Thermal conductivity of 316L powders increases with powder packing densification	[117]

Table 5: Effects of Powder Granulometry on Part Performance

Part Characteristic	Key Findings	Reference
Part Density	• Negatively skewed 316L powder which contained fine particles obtained higher part densities at a specific energy density range and lower layer thickness over finer *Gaussian* grade. Finest granulometry powder was observed with the best densification results.	[55]
	• Wider distributed 316L powder produced higher part densities as compared to the narrower grade	[75]
Mechanical Properties	• Negatively skewed 316L grade showed higher ductility but lower tensile strength as compared to *Gaussian* distributed powders	[55]
	• Narrower distributed 316L powder produced higher part mechanical strength but smaller elongation over wider distributed grade	[75]
	• Comparable tensile strength observed between bimodal Ti6Al4V powder and monomodal grades	[74]
Microstructure	• Higher martensitic content observed in finer PH 17-4 powder (D_{90}<16µm) as compared to coarser grade (D_{90}<25µm)	[132]
	• Finer dendritic structure observed in bimodal Al-Si powder as compared to *Gaussian* and Tri-modal grades	[73]
Surface Quality	• 316L powder with finest granulometry (**D_{90}** = 24.17µm) obtained the best surface quality	[55]
	• Wider distributed powder (0-45µm) exhibited better side surface roughness as compared to narrower grade (10-45µm)	[75]

7.0 Outlook

Extensive research work related to the study of metal AM feedstock characteristics, not limited to granulometry, is still required to strengthen the understanding of material-process variation in order to improve repeatability and reliability in SLM manufacture:

(1) Mapping of suitable powder size distribution range to process windows which provides optimum powder behaviour as well as part quality for different materials

(2) Quantification studies on powder surface area to understand the effects on contamination (E.g. oxygen content) and irradiation (E.g. thermal absorptivity) relative to powder size attributes

(3) Improve on existing characterisation techniques and establish standards specifically for metal AM powders to qualify feedstock quality governed by morphology, granulometry, surface chemistry, packing density, flowability and thermal properties

(4) Design in-situ metrology approaches to determine feedstock behaviour within the process chamber (E.g. powder bed scanning with dynamic image analysis) and ensure conforming powder granulometry

(5) Further investigate on the effects of powder characteristics variation on mechanical properties and microstructure as well as build failures which transit into part defects including porosity, distortions and surface quality

Acknowledgements

Mr. Tan Jun Hao wishes to acknowledge the Postgraduate Research Studentship provided by School of Engineering, Newcastle University for the funding of his PhD research study under Newcastle University Singapore.

References

[1] D.D. Gu, W. Meiners, K. Wissenbach, R. Poprawe, Laser additive manufacturing of metallic components: materials, processes and mechanisms, Int. Mater. Rev. 57 (2012) 133–164. doi:10.1179/1743280411Y.0000000014.

[2] M. Seifi, A. Salem, J. Beuth, O. Harrysson, J.J. Lewandowski, Overview of Materials Qualification Needs for Metal Additive Manufacturing, Jom. 68 (2016) 747–764. doi:10.1007/s11837-015-1810-0.

[3] L.E. Murr, S.M. Gaytan, D.A. Ramirez, E. Martinez, J. Hernandez, K.N. Amato, P.W. Shindo, F.R. Medina, R.B. Wicker, Metal Fabrication by Additive Manufacturing Using Laser and Electron Beam Melting Technologies, J. Mater. Sci. Technol. 28 (2012) 1–14. doi:10.1016/S1005-0302(12)60016-4.

[4] E. Herderick, Additive manufacturing of metals: A review, Mater. Sci. Technol. Conf. Exhib. 2011, MS T'11. 2 (2011) 1413–1425. http://www.scopus.com/inward/record.url?eid=2-s2.0-84856301323&partnerID=40&md5=e02018d10b2ca37a7e2ae1773e4fcaec.

[5] M. Król, L. Dobrzański, I. Reimann, Surface quality in selective laser melting of metal powders, Arch. Mater. Sci. 60 (2013) 87–92. http://www.doaj.org/doaj?func=fulltext&aId=1488627.

[6] E. Liverani, S. Toschi, L. Ceschini, A. Fortunato, Effect of selective laser melting (SLM) process parameters on microstructure and mechanical properties of 316L austenitic stainless steel, J. Mater. Process. Technol. 249 (2017) 255–263. doi:10.1016/j.jmatprotec.2017.05.042.

[7] J. Sun, Y. Yang, D. Wang, Parametric optimization of selective laser melting for forming

Ti6Al4V samples by Taguchi method, Opt. Laser Technol. 49 (2013) 118–124. doi:10.1016/j.optlastec.2012.12.002.

[8] Z. Hu, H. Zhu, H. Zhang, X. Zeng, Experimental investigation on selective laser melting of 17-4PH stainless steel, Opt. Laser Technol. 87 (2017) 17–25. doi:10.1016/j.optlastec.2016.07.012.

[9] W.J. Sames, F.A. List, S. Pannala, R.R. Dehoff, S.S. Babu, The metallurgy and processing science of metal additive manufacturing, Int. Mater. Rev. 6608 (2016) 1–46. doi:10.1080/09506608.2015.1116649.

[10] R.J. Hebert, Viewpoint: Metallurgical Aspects Of Powder Bed Metal Additive Manufacturing, J. Mater. Sci. 51 (2016) 1165–1175. doi:10.1007/s10853-015-9479-x.

[11] D. Herzog, V. Seyda, E. Wycisk, C. Emmelmann, Additive manufacturing of metals, Acta Mater. 117 (2016) 371–392. doi:10.1016/j.actamat.2016.07.019.

[12] C.Y. Yap, C.K. Chua, Z.L. Dong, Z.H. Liu, D.Q. Zhang, L.E. Loh, S.L. Sing, Review of selective laser melting: Materials and applications, Appl. Phys. Rev. 2 (2015) 0–21. doi:10.1063/1.4935926.

[13] J.P. Kruth, M. Badrossamay, E. Yasa, J. Deckers, L. Thijs, J. Van Humbeeck, M. Badrosamay, E. Yasa, J. Deckers, L. Thijs, J. Van Humbeeck, Part and material properties in selective laser melting of metals, 16th Int. Symp. Electromachining. (2010) 1–12.

[14] W.E. King, A.T. Anderson, R.M. Ferencz, N.E. Hodge, C. Kamath, S.A. Khairallah, A.M. Rubenchik, Laser powder bed fusion additive manufacturing of metals; physics, computational, and materials challenges, Appl. Phys. Rev. 2 (2015) 41304. doi:10.1063/1.4937809.

[15] R.M. German, Prediction of sintered density for bimodal powder mixtures, Metall. Trans. A. 23 (1992) 1455–1465. doi:10.1007/BF02647329.

[16] B.J. Dawes, R. Bowerman, Introduction to the Additive Manufacturing Powder Metallurgy Supply Chain, Johnson Matthey Technol. Rev. 59 (2015) 243–256. doi:http://dx.doi.org/10.1595/205651315X688686.

[17] J.M. Benson, E. Snyders, The Need for Powder Characterisation in the Additive Manufacturing, South African J. Ind. Eng. 26 (2015) 104–114.

[18] A. Popovich, V. Sufiiarov, Metal Powder Additive Manufacturing, in: New Trends 3D Print., 2016. doi:10.5772/63337.

[19] J.A. Slotwinski, E.J. Garboczi, Metrology Needs for Metal Additive Manufacturing Powders, Jom. 67 (2015) 538–543. doi:10.1007/s11837-014-1290-7.

[20] J. Cooke, A., & Slotwinski, Properties of metal powders for additive manufacturing: a review of the state of the art of metal powder property testing., (2012).

[21] S.M. Yusuf, N. Gao, Influence of energy density on metallurgy and properties in metal additive manufacturing, Mater. Sci. Technol. 836 (2017) 1–21. doi:10.1080/02670836.2017.1289444.

[22] B. Zhang, C. Coddet, Selective Laser Melting of Iron Powder: Observation of Melting Mechanism and Densification Behavior Via Point-Track-Surface-Part Research, J. Manuf. Sci. Eng. 138 (2015) 51001. doi:10.1115/1.4031366.

[23] L. Thijs, F. Verhaeghe, T. Craeghs, J. Van Humbeeck, J.P. Kruth, A study of the microstructural evolution during selective laser melting of Ti-6Al-4V, Acta Mater. 58 (2010) 3303–3312. doi:10.1016/j.actamat.2010.02.004.

[24] E. Louvis, P. Fox, C.J. Sutcliffe, Selective laser melting of aluminium components, J. Mater. Process. Technol. 211 (2011) 275–284. doi:10.1016/j.jmatprotec.2010.09.019.

[25] Z. Wang, K. Guan, M. Gao, X. Li, X. Chen, X. Zeng, The microstructure and mechanical properties of deposited-IN718 by selective laser melting, J. Alloys Compd. 513 (2012) 518–

523. doi:10.1016/j.jallcom.2011.10.107.

[26] J.A. Cherry, H.M. Davies, S. Mehmood, N.P. Lavery, S.G.R. Brown, J. Sienz, Investigation into the effect of process parameters on microstructural and physical properties of 316L stainless steel parts by selective laser melting, Int. J. Adv. Manuf. Technol. 76 (2014) 869–879. doi:10.1007/s00170-014-6297-2.

[27] Z. Sun, X. Tan, S.B. Tor, W.Y. Yeong, Selective laser melting of stainless steel 316L with low porosity and high build rates, Mater. Des. 104 (2016) 197–204. doi:10.1016/j.matdes.2016.05.035.

[28] D. Wang, C. Song, Y. Yang, Y. Bai, Investigation of crystal growth mechanism during selective laser melting and mechanical property characterization of 316L stainless steel parts, Mater. Des. 100 (2016) 291–299. doi:10.1016/j.matdes.2016.03.111.

[29] P. Fischer, V. Romano, H.P. Weber, N.P. Karapatis, E. Boillat, R. Glardon, Sintering of commercially pure titanium powder with a Nd:YAG laser source, Acta Mater. 51 (2003) 1651–1662. doi:10.1016/S1359-6454(02)00567-0.

[30] J.P. Kruth, G. Levy, F. Klocke, T.H.C. Childs, Consolidation phenomena in laser and powder-bed based layered manufacturing, CIRP Ann. - Manuf. Technol. 56 (2007) 730–759. doi:10.1016/j.cirp.2007.10.004.

[31] M. Rombouts, J.P. Kruth, L. Froyen, P. Merce, Fundamentals of Selective Laser Melting of alloyed steel powders Fundamentals of Selective Laser Melting of alloyed steel powders, CIRP Ann. - Manuf. Technol. 55 (2006) 187–192.

[32] B. Song, S. Dong, S. Deng, H. Liao, C. Coddet, Microstructure and tensile properties of iron parts fabricated by selective laser melting, Opt. Laser Technol. 56 (2014) 451–460. doi:http://dx.doi.org/10.1016/j.optlastec.2013.09.017.

[33] P. Mercelis, J. Kruth, Residual stresses in selective laser sintering and selective laser melting, Rapid Prototyp. J. 12 (2006) 254–265. doi:10.1108/13552540610707013.

[34] M. Shiomi, K. Osakada, K. Nakamura, T. Yamashita, F. Abe, Residual Stress within Metallic Model Made by Selective Laser Melting Process, CIRP Ann. - Manuf. Technol. 53 (2004) 195–198. doi:10.1016/S0007-8506(07)60677-5.

[35] E. Brinksmeier, G. Levy, D. Meyer, A.B. Spierings, Surface integrity of selective-laser-melted components, CIRP Ann. - Manuf. Technol. 59 (2010) 601–606. doi:10.1016/j.cirp.2010.03.131.

[36] C. Li, J.F. Liu, Y.B. Guo, Prediction of Residual Stress and Part Distortion in Selective Laser Melting, Procedia CIRP. 45 (2016) 171–174. doi:10.1016/j.procir.2016.02.058.

[37] H. Ali, L. Ma, H. Ghadbeigi, K. Mumtaz, In-situ residual stress reduction, martensitic decomposition and mechanical properties enhancement through high temperature powder bed pre-heating of Selective Laser Melted Ti6Al4V, Mater. Sci. Eng. A. 695 (2017) 211–220. doi:10.1016/j.msea.2017.04.033.

[38] K. Kempen, B. Vrancken, L. Thijs, S. Buls, J. Van Humbeeck, J.-P. Kruth, Lowering thermal gradients in Selective Laser melting by pre-heating the baseplate, Solid Free. Fabr. Proc. 24 (2013). doi:10.1017/CBO9781107415324.004.

[39] J.-P. Kruth, J. Deckers, E. Yasa, R. Wauthle, Assessing and comparing influencing factors of residual stresses in selective laser melting using a novel analysis method, Proc. Inst. Mech. Eng. Part B J. Eng. Manuf. 226 (2012) 980–991. doi:10.1177/0954405412437085.

[40] R. Li, J. Liu, Y. Shi, L. Wang, W. Jiang, Balling behavior of stainless steel and nickel powder during selective laser melting process, Int. J. Adv. Manuf. Technol. 59 (2012) 1025–1035. doi:10.1007/s00170-011-3566-1.

[41] D. Gu, Y. Shen, Balling phenomena in direct laser sintering of stainless steel powder: Metallurgical mechanisms and control methods, Mater. Des. 30 (2009) 2903–2910.

doi:10.1016/j.matdes.2009.01.013.

[42] K. Antony, N. Arivazhagan, Studies on energy penetration and marangoni effect during laser melting process, J. Eng. Sci. Technol. 10 (2015) 509–525.

[43] E. Yasa, J. Deckers, J. Kruth, The investigation of the influence of laser re-melting on density, surface quality and microstructure of selective laser melting parts, Rapid Prototyp. J. 17 (2011) 312–327. doi:10.1108/13552541111156450.

[44] W.E. King, H.D. Barth, V.M. Castillo, G.F. Gallegos, J.W. Gibbs, D.E. Hahn, C. Kamath, A.M. Rubenchik, Observation of keyhole-mode laser melting in laser powder-bed fusion additive manufacturing, J. Mater. Process. Technol. 214 (2014) 2915–2925. doi:10.1016/j.jmatprotec.2014.06.005.

[45] B. Song, S. Dong, Q. Liu, H. Liao, C. Coddet, Vacuum heat treatment of iron parts produced by selective laser melting: Microstructure, residual stress and tensile behavior, Mater. Des. 54 (2014) 727–733. doi:10.1016/j.matdes.2013.08.085.

[46] H. Gong, K. Rafi, H. Gu, T. Starr, B. Stucker, Analysis of defect generation in Ti-6Al-4V parts made using powder bed fusion additive manufacturing processes, Addit. Manuf. 1 (2014) 87–98. doi:10.1016/j.addma.2014.08.002.

[47] Y. Liu, Y. Yang, S. Mai, D. Wang, C. Song, Investigation into spatter behavior during selective laser melting of AISI 316L stainless steel powder, Mater. Des. 87 (2015) 797–806. doi:10.1016/j.matdes.2015.08.086.

[48] B. Engel, D.L. Bourell, Titanium alloy powder preparation for selective laser sintering, Rapid Prototyp. J. 6 (2000) 97–106. doi:10.1108/13552540010323574.

[49] B. Vrancken, L. Thijs, J.-P. Kruth, J. Van Humbeeck, Heat treatment of Ti6Al4V produced by Selective Laser Melting: Microstructure and mechanical properties, J. Alloys Compd. 541 (2012) 177–185. doi:10.1016/j.jallcom.2012.07.022.

[50] B. Vrancken, L. Thijs, J.P. Kruth, J. Van Humbeeck, Microstructure and mechanical properties of a novel β titanium metallic composite by selective laser melting, Acta Mater. 68 (2014) 150–158. doi:10.1016/j.actamat.2014.01.018.

[51] J. Karlsson, A. Snis, H. Engqvist, J. Lausmaa, Characterization and comparison of materials produced by Electron Beam Melting (EBM) of two different Ti-6Al-4V powder fractions, J. Mater. Process. Technol. 213 (2013) 2109–2118. doi:10.1016/j.jmatprotec.2013.06.010.

[52] S. Hoeges, A. Zwiren, C. Schade, Additive manufacturing using water atomized steel powders, Met. Powder Rep. 72 (2017) 111–117. doi:10.1016/j.mprp.2017.01.004.

[53] M. Boisvert, D. Christopherson, P. Beaulieu, G. L'Espérance, Treatment of ferrous melts for the improvement of the sphericity of water atomized powders, Mater. Des. 116 (2017) 644–655. doi:10.1016/j.matdes.2016.12.059.

[54] C.T. Schade, T.F. Murphy, C. Walton, Development of atomized powders for additive manufacturing, World Congr. Powder Metall. Part. Mater. PM 2014, May 18, 2014 - May 22, 2014. (2014) 215–226.

[55] S. Dietrich, M. Wunderer, A. Huissel, M.F. Zaeh, A New Approach for a Flexible Powder Production for Additive Manufacturing, Procedia Manuf. 6 (2016) 88–95. doi:10.1016/j.promfg.2016.11.012.

[56] R. Li, Y. Shi, Z. Wang, L. Wang, J. Liu, W. Jiang, Densification behavior of gas and water atomized 316L stainless steel powder during selective laser melting, Appl. Surf. Sci. 256 (2010) 4350–4356. doi:10.1016/j.apsusc.2010.02.030.

[57] C. Kamath, B. El-Dasher, G.F. Gallegos, W.E. King, A. Sisto, Density of additively-manufactured, 316L SS parts using laser powder-bed fusion at powers up to 400 W, Int. J. Adv. Manuf. Technol. 74 (2014) 65–78. doi:10.1007/s00170-014-5954-9.

[58] A.B. Spierings, G. Levy, Comparison of density of stainless steel 316L parts produced with

selective laser melting using different powder grades, Solid Free. Fabr. Proc. (2009) 342–353.

[59] P. Hanzl, M. Zetek, T. Bakša, T. Kroupa, The influence of processing parameters on the mechanical properties of SLM parts, in: Procedia Eng., 2015: pp. 1405–1413. doi:10.1016/j.proeng.2015.01.510.

[60] J.A. Slotwinski, E.J. Garboczi, P.E. Stutzman, C.F. Ferraris, S.S. Watson, M.A. Peltz, Characterization of Metal Powders Used for Additive Manufacturing., J. Res. Natl. Inst. Stand. Technol. 119 (2014) 460–93. doi:10.6028/jres.119.018.

[61] J. Clayton, D. Millington-Smith, B. Armstrong, The Application of Powder Rheology in Additive Manufacturing, Jom. 67 (2015) 544–548. doi:10.1007/s11837-015-1293-z.

[62] A.B. Spierings, M. Voegtlin, T. Bauer, K. Wegener, Powder flowability characterisation methodology for powder-bed-based metal additive manufacturing, Prog. Addit. Manuf. 1 (2016) 9–20. doi:10.1007/s40964-015-0001-4.

[63] A. Strondl, O. Lyckfeldt, H. Brodin, U. Ackelid, Characterization and Control of Powder Properties for Additive Manufacturing, Jom. 67 (2015) 549–554. doi:10.1007/s11837-015-1304-0.

[64] H.P. Tang, M. Qian, N. Liu, X.Z. Zhang, G.Y. Yang, J. Wang, Effect of Powder Reuse Times on Additive Manufacturing of Ti-6Al-4V by Selective Electron Beam Melting, JOM. 67 (2015) 555–563. doi:10.1007/s11837-015-1300-4.

[65] L.C. Ardila, F. Garciandia, J.B. González-Díaz, P. Álvarez, A. Echeverria, M.M. Petite, R. Deffley, J. Ochoa, Effect of IN718 recycled powder reuse on properties of parts manufactured by means of Selective Laser Melting, Phys. Procedia. 56 (2014) 99–107. doi:10.1016/j.phpro.2014.08.152.

[66] ASTM B243-13, Standard Terminology of Powder Metallurgy, ASTM Int. (2014) 1–12. doi:10.1520/B0243-13.1.

[67] E.O. Olakanmi, Effect of mixing time on the bed density, and microstructure of selective laser sintered (sls) aluminium powders, Mater. Res. 15 (2012) 167–176. doi:10.1590/S1516-14392012005000031.

[68] P.W. Cleary, M.L. Sawley, DEM modelling of industrial granular flows: 3D case studies and the effect of particle shape on hopper discharge, Appl. Math. Model. 26 (2002) 89–111. doi:10.1016/S0307-904X(01)00050-6.

[69] G. Egger, P.E. Gygax, R. Glardon, N.P. Karapatis, Optimization of powder layer density in selective laser sintering, 10th Solid Free. Fabr. Symp. (1999) 255–263. http://infoscience.epfl.ch/record/153069.

[70] R.M. German, Powder Metallurgy Science (Second Edition), 1994.

[71] H. Irrinki, M. Dexter, B. Barmore, R. Enneti, S. Pasebani, S. Badwe, J. Stitzel, R. Malhotra, S. V. Atre, Effects of Powder Attributes and Laser Powder Bed Fusion (L-PBF) Process Conditions on the Densification and Mechanical Properties of 17-4 PH Stainless Steel, Jom. 68 (2016) 860–868. doi:10.1007/s11837-015-1770-4.

[72] ASTM B214-07, Standard Test Method for Sieve Analysis of Metal Powders, ASTM Int. (2011).

[73] A. B822-10, Standard Test Method for Particle Size Distribution of Metal Powders and Related Compounds by Light Scattering, ASTM Int. (n.d.).

[74] A. Jillavenkatesa, S.J. Dapkunas, L.-S.H. Lum, Particle Size Characterization, NIST Spec. Publ. 960 (2001) 164. doi:Particle size characterization.

[75] ISO 13322-2 2006, Particle Size Analysis—Image Analysis Methods—Part 2: Dynamic Image Analysis Methods, Geneva Int. Organ. Stand. (2006).

[76] Malvern Instruments, Morphologi G3, (n.d.). https://www.malvern.com/en/products/product-range/morphologi-range/morphologi-g3.

[77] R. Technology, Dynamic Image Analysis, Camsizer XT, (n.d.). http://www.retsch-technology.com/rt/products/dynamic-imageanalysis/camsizer-xt.

[78] R. Engeli, T. Etter, S. Hövel, K. Wegener, Processability of different IN738LC powder batches by selective laser melting, J. Mater. Process. Technol. 229 (2016) 484–491. doi:10.1016/j.jmatprotec.2015.09.046.

[79] A.B. Spierings, N. Herres, G. Levy, Influence of the particle size distribution on surface quality and mechanical properties in AM steel parts, Rapid Prototyp. J. 17 (2011) 195–202. doi:10.1108/13552541111124770.

[80] C.C. Ng, M.M. Savalani, M.L. Lau, H.C. Man, Microstructure and mechanical properties of selective laser melted magnesium, Appl. Surf. Sci. 257 (2011) 7447–7454. doi:10.1016/j.apsusc.2011.03.004.

[81] M. Simonelli, C. Tuck, N.T. Aboulkhair, I. Maskery, I. Ashcroft, R.D. Wildman, R. Hague, A Study on the Laser Spatter and the Oxidation Reactions During Selective Laser Melting of 316L Stainless Steel, Al-Si10-Mg, and Ti-6Al-4V, Metall. Mater. Trans. A Phys. Metall. Mater. Sci. 46 (2015) 3842–3851. doi:10.1007/s11661-015-2882-8.

[82] T. Starr, K. Rafi, B. Stucker, C. Scherzer, Controlling phase composition in selective laser melted stainless steels, Proc. Solid Free. Fabr. Symp. (2012) 439–446.

[83] A. Hodgson, S. Haq, Water adsorption and the wetting of metal surfaces, Surf. Sci. Rep. 64 (2009) 381–451. doi:10.1016/j.surfrep.2009.07.001.

[84] V. Karde, C. Ghoroi, Fine powder flow under humid environmental conditions from the perspective of surface energy, Int. J. Pharm. 485 (2015) 192–201. doi:10.1016/j.ijpharm.2015.03.021.

[85] B. Liu, R. Wildman, C. Tuck, I. Ashcroft, R. Hague, Investigation the Effect of Particle Size Distribution on Processing Parameters Optimisation in Selective Laser Melting Process, Sff. (2011) 227–238. doi:10.1017/CBO9781107415324.004.

[86] R.W. Daryl, Particle Engineering in Pharmaceutical Solids Processing: Surface Energy Considerations, Curr. Pharm. Des. 21 (2015) 2677–2694. doi:http://dx.doi.org/10.2174/1381612821666150416100319.

[87] T. Young, An Essay on the Cohesion of Fluids, Philos. Trans. R. Soc. London. 95 (1805) 65–87. doi:10.1098/rstl.1805.0005.

[88] V. Bérard, E. Lesniewska, C. Andrès, D. Pertuy, C. Laroche, Y. Pourcelot, Affinity scale between a carrier and a drug in DPI studied by atomic force microscopy, Int. J. Pharm. 247 (2002) 127–137. doi:10.1016/S0378-5173(02)00400-3.

[89] J.M. Oh, B.G. Lee, S.W. Cho, S.W. Lee, G.S. Choi, J.W. Lim, Oxygen effects on the mechanical properties and lattice strain of Ti and Ti-6Al-4V, Met. Mater. Int. 17 (2011) 733–736. doi:10.1007/s12540-011-1006-2.

[90] X.P. Li, K.M. O'Donnell, T.B. Sercombe, Selective laser melting of Al-12Si alloy: Enhanced densification via powder drying, Addit. Manuf. 10 (2016) 10–14. doi:10.1016/j.addma.2016.01.003.

[91] T. Marcu, M. Todea, I. Gligor, P. Berce, C. Popa, Effect of surface conditioning on the flowability of Ti6Al7Nb powder for selective laser melting applications, Appl. Surf. Sci. 258 (2012) 3276–3282. doi:10.1016/j.apsusc.2011.11.081.

[92] J.P. Kruth, L. Froyen, J. Van Vaerenbergh, P. Mercelis, M. Rombouts, B. Lauwers, Selective laser melting of iron-based powder, J. Mater. Process. Technol. 149 (2004) 616–622. doi:10.1016/j.jmatprotec.2003.11.051.

[93] A. Simchi, H. Pohl, Direct laser sintering of iron-graphite powder mixture, Mater. Sci. Eng. A. 383 (2004) 191–200. doi:10.1016/j.msea.2004.05.070.

[94] R. O'Leary, R. Setchi, P. Prickett, G. Hankins, N. Jones, An Investigation into the Recycling

of Ti-6Al-4V Powder Used Within SLM to Improve Sustainability, SDM'2015 2nd Int. Conf. Sustain. Des. Manuf. ,. (2015) 14–17.

[95] R.M. German, Particle packing characteristics, Princeton, N.J. : Metal Powder Industries Federation, 1989.

[96] F. j. Gürtler, M. Karg, M. Dobler, S. Kohl, I. Tzivilsky3, M. Schmidt, Influence of powder distribution on process stability in laser beam melting: Analysis of melt pool dynamics by numerical simulations, Solid Free. Symp. Texas. (2014) 1099–1117.

[97] A. Zocca, C.M. Gomes, T. M??hler, J. G??nster, Powder-bed stabilization for powder-based additive manufacturing, Adv. Mech. Eng. 2014 (2014). doi:10.1155/2014/491581.

[98] F.-J. Gürtler, M. Karg, K.-H. Leitz, M. Schmidt, Simulation of Laser Beam Melting of Steel Powders using the Three-Dimensional Volume of Fluid Method, Phys. Procedia. 41 (2013) 881–886. doi:10.1016/j.phpro.2013.03.162.

[99] P. Meakin, R. Jullien, Restructuring effects in the rain model for random deposition, J. Phys. 48 (1987) 1651–1662. doi:10.1051/jphys:0198700480100165100.

[100] Y.S. Lee, W. Zhang, Mesoscopic Simulation of Heat Transfer and Fluid Flow in Laser Powder Bed Additive Manufacturing, Int. Solid Free Form Fabr. Symp. Austin. (2015) 1154–1165. http://sffsymposium.engr.utexas.edu/sites/default/files/2015/2015-94-Lee.pdf.

[101] C. Körner, E. Attar, P. Heinl, Mesoscopic simulation of selective beam melting processes, J. Mater. Process. Technol. 211 (2011) 978–987. doi:10.1016/j.jmatprotec.2010.12.016.

[102] G. Jacob, A. Donmez, J. Slotwinski, S. Moylan, Measurement of powder bed density in powder bed fusion additive manufacturing processes, Meas. Sci. Technol. 27 (2016) 115601. doi:10.1088/0957-0233/27/11/115601.

[103] H. Gu, H. Gong, J.J.S. Dilip, D. Pal, A. Hicks, H. Doak, B. Stucker, Effects of Powder Variation on the Microstructure and Tensile Strength of Ti6Al4V Parts Fabricated by Selective Laser Melting, Solid Free. Fabr. Symp. (2014) 470–483.

[104] A.M. Elliott, P. Nandwana, D. Siddel, B.G. Compton, A Method for Measuring Powder Bed Density in Binder Jet Additive Manufacturing Process and the Powder Feedstock Characteristics Influencing the Powder Bed Density, Solid Free. Fabr. 2016. Proceeding (2016) 1031–1037.

[105] E.O. Olakanmi, K.W. Dalgarno, R.F. Cochrane, Laser sintering of blended Al-Si powders, Rapid Prototyp. J. 18 (2012) 109–119. doi:doi:10.1108/13552541211212096.

[106] A. Castellanos, The relationship between attractive interparticle forces and bulk behaviour in dry and uncharged fine powders, 2005. doi:10.1080/17461390500402657.

[107] M. Krantz, H. Zhang, J. Zhu, Characterization of powder flow: Static and dynamic testing, Powder Technol. 194 (2009) 239–245. doi:10.1016/j.powtec.2009.05.001.

[108] A.B. Yu, J.S. Hall, Packing of fine powders subjected to tapping, Powder Technol. 78 (1994) 247–256. doi:10.1016/0032-5910(93)02790-H.

[109] E. Yasa, J.P. Kruth, J. Deckers, Manufacturing by combining Selective Laser Melting and Selective Laser Erosion/laser re-melting, CIRP Ann. - Manuf. Technol. 60 (2011) 263–266. doi:10.1016/j.cirp.2011.03.063.

[110] ASTM D7481-09, Standard test methods for determining loose and tapped bulk densities of powders using a graduated cylinder, Annu. B. ASTM Stand. (2009) 1–4. doi:10.1520/D7481-09.1.

[111] E.C. Abdullah, D. Geldart, The use of bulk density measurements as flowability indicators, Powder Technol. 102 (1999) 151–165. doi:10.1016/S0032-5910(98)00208-3.

[112] ASTM B213-17, Standard Test Methods for Flow Rate of Metal Powders Using the Hall Flowmeter, ASTM Int. i (2014) 213–216. doi:10.1520/B0213-13.2.

[113] D. Geldart, E.C. Abdullah, A. Hassanpour, L.C. Nwoke, I. Wouters, Characterization of powder flowability using measurement of angle of repose, China Particuology. 4 (2006) 104–107. doi:10.1016/S1672-2515(07)60247-4.

[114] D. Schulze, Flow properties of powders and bulk solids, Braunschweig/Wolfenbu Ttel, Ger. Univ. …. (2006) 1–21. http://dietmar-schulze.de/grdle1.pdf.

[115] R. Freeman, Measuring the flow properties of consolidated, conditioned and aerated powders - A comparative study using a powder rheometer and a rotational shear cell, Powder Technol. 174 (2007) 25–33. doi:10.1016/j.powtec.2006.10.016.

[116] J. Clayton, Optimising metal powders for additive manufacturing, Met. Powder Rep. 69 (2014) 14–17. doi:10.1016/S0026-0657(14)70223-1.

[117] I. Yadroitsev, A. Gusarov, I. Yadroitsava, I. Smurov, Single track formation in selective laser melting of metal powders, J. Mater. Process. Technol. 210 (2010) 1624–1631. doi:10.1016/j.jmatprotec.2010.05.010.

[118] A. Streek, P. Regenfuss, H. Exner, Fundamentals of energy conversion and dissipation in powder layers during laser micro sintering, in: Phys. Procedia, 2013: pp. 858–869. doi:10.1016/j.phpro.2013.03.159.

[119] A. Foroozmehr, M. Badrossamay, E. Foroozmehr, S. Golabi, Finite Element Simulation of Selective Laser Melting process considering Optical Penetration Depth of laser in powder bed, Mater. Des. 89 (2016) 255–263. doi:10.1016/j.matdes.2015.10.002.

[120] P. Fischer, N. Karapatis, V. Romano, R. Glardon, H.P. Weber, A model for the interaction of near-infrared laser pulses with metal powders in selective laser sintering, Appl. Phys. a-Materials Sci. Process. 74 (2002) 467–474. doi:10.1007/s003390101139.

[121] R.W. McVey, R.M. Melnychuk, J. a. Todd, R.P. Martukanitz, Absorption of laser irradiation in a porous powder layer, J. Laser Appl. 19 (2007) 214. doi:10.2351/1.2756854.

[122] N.K. Tolochko, T. Laoui, Y. V Khlopkov, S.E. Mozzharov, V.I. Titov, M.B. Ignatiev, Absorptance of powder materials suitable for laser sintering, Rapid Prototyp. J. 6 (2000) 155–160. doi:Doi 10.1108/13552540010337029.

[123] A. V. Gusarov, I. Smurov, Modeling the interaction of laser radiation with powder bed at selective laser melting, in: Phys. Procedia, 2010: pp. 381–394. doi:10.1016/j.phpro.2010.08.065.

[124] C.D. Boley, S.A. Khairallah, A.M. Rubenchik, Calculation of laser absorption by metal powders in additive manufacturing., Appl. Opt. 54 (2015) 2477–82. doi:10.1364/AO.54.002477.

[125] X. Wang, J. Kruth, Energy absorption and penetration in selective laser sintering: a ray tracing model, Proc. Int. Conf. Math. Model. Simul. Met. Technol. (2000) 673–683. http://www.ariel.ac.il/sites/conf/mmt/MMT-2000/papers/673-682.doc.

[126] A. Rubenchik, S. Wu, S. Mitchell, I. Golosker, M. LeBlanc, N. Peterson, Direct measurements of temperature-dependent laser absorptivity of metal powders, Appl. Opt. 54 (2015) 7230. doi:10.1364/AO.54.007230.

[127] S.S. Sih, J.W. Barlow, The Measurement of the Thermal Properties and Absorptances of Powders Near Their Melting Temperatures, Chem. Eng. (1992) 131–140.

[128] W.J. Parker, R.J. Jenkins, C.P. Butler, G.L. Abbott, Flash method of determining thermal diffusivity, heat capacity, and thermal conductivity, J. Appl. Phys. 32 (1961) 1679–1684. doi:10.1063/1.1728417.

[129] ASTM International, E1461. Standard test method for thermal diffusivity by the flash method., 2013. doi:10.1520/E1461-13.

[130] J. Romano, L. Ladani, M. Sadowski, Thermal Modeling of Laser Based Additive Manufacturing Processes within Common Materials, Procedia Manuf. 1 (2015) 238–250.

doi:10.1016/j.promfg.2015.09.012.

[131] B. Schoinochoritis, D. Chantzis, K. Salonitis, Simulation of metallic powder bed additive manufacturing processes with the finite element method: A critical review, Proc. Inst. Mech. Eng. Part B J. Eng. Manuf. (2015) 1–22. doi:10.1177/0954405414567522.

[132] S. Lowell, J.E. Shields, M.A. Thomas, M. Thommes, Characterization of Porous Solids and Powders: Surface Area, Pore Size and Density, 2004. doi:10.1007/978-1-4020-2303-3.

[133] A. Simchi, The role of particle size on the laser sintering of iron powder, Metall. Mater. Trans. B. 35 (2004) 937–948. doi:10.1007/s11663-004-0088-3.

[134] S. Liu, Z. Ha, Prediction of random packing limit for multimodal particle mixtures, Powder Technol. 126 (2002) 283–296. doi:10.1016/S0032-5910(02)00075-X.

[135] J.E. Funk, D. Dinger, Predictive Process Control of Crowded Particulate Suspensions, 1st ed., Springer US, 1994. doi:10.1007/978-1-4615-3118-0.

[136] C.C. Furnas, Grading aggregates I-Mathematical relations for beds of broken solids of maximum density, Ind. Eng. Chem. Res. 23 (1931) 1052–1058. doi:10.1021/ie50261a017.

[137] A.E.R. Westman, THE PACKING OF PARTICLES: EMPIRICAL EQUATIONS FOR INTERMEDIATE DIAMETER RATIOS, J. Am. Ceram. Soc. 19 (1936) 127–129. doi:10.1111/j.1151-2916.1936.tb19809.x.

[138] A.H.. Andreasen, J. Andersen, Relation between grain size and interstitial space in products of unconsolidated granules, Kolloid-Zeitschrift. 50 (1930) pp.217-228.

[139] G.P. Bierwagen, T.E. Sanders, Studies of the Effects of Particle Size Distribution on the Packing Efficiency of Particles, Powder Technol. 10 (1974) 111–119. doi:10.1016/0032-5910(74)80036-7.

[140] G.T. Nolan, P.E. Kavanagh, Size distribution of interstices in random packings of spheres, Powder Technol. 78 (1994) 231–238. doi:10.1016/0032-5910(93)02789-D.

[141] R.K. McGeary, Mechanical Packing of Spherical Particles, J. Am. Ceram. Soc. 44 (1961) 513–522. doi:10.1111/j.1151-2916.1961.tb13716.x.

[142] H.H. Zhu, J.Y.H. Fuh, L. Lu, The influence of powder apparent density on the density in direct laser-sintered metallic parts, Int. J. Mach. Tools Manuf. 47 (2007) 294–298. doi:10.1016/j.ijmachtools.2006.03.019.

[143] A.C.S.M. James P. Bennett, Jeffery D. Smith, Fundamentals of refractory technology: proceedings of the Refractory Ceramics Division Focused Lecture Series presented at the 101st and 102nd Annual Meetings held April 25-28, 1999, in Indianapolis, Indiana, and April 30-May 3, 2000, in St. Louis, Missou, American Ceramic Society, 2007.

[144] M. Rombouts, L. Froyen, A. V. Gusarov, E.H. Bentefour, C. Glorieux, Photopyroelectric measurement of thermal conductivity of metallic powders, J. Appl. Phys. 97 (2005). doi:10.1063/1.1832740.

[145] A. V. Gusarov, T. Laoui, L. Froyen, V.I. Titov, Contact thermal conductivity of a powder bed in selective laser sintering, Int. J. Heat Mass Transf. 46 (2003) 1103–1109. doi:10.1016/S0017-9310(02)00370-8.

[146] J. Zhou, Y. Zhang, J.K. Chen, Numerical Simulation of Random Packing of Spherical Particles for Powder-Based Additive Manufacturing, J. Manuf. Sci. Eng. 131 (2009) 31004. doi:10.1115/1.3123324.

[147] G. Tapia, A.H. Elwany, H. Sang, Prediction of porosity in metal-based additive manufacturing using spatial Gaussian process models, Addit. Manuf. 12 (2016) 282–290. doi:10.1016/j.addma.2016.05.009.

[148] T.M. Mower, M.J. Long, Mechanical behavior of additive manufactured, powder-bed laser-fused materials, Mater. Sci. Eng. A. 651 (2016) 198–213. doi:10.1016/j.msea.2015.10.068.

[149] B. Song, X. Zhao, S. Li, C. Han, Q. Wei, S. Wen, J. Liu, Y. Shi, Differences in microstructure and properties between selective laser melting and traditional manufacturing for fabrication of metal parts: A review, Front. Mech. Eng. 10 (2015) 111–125. doi:10.1007/s11465-015-0341-2.

[150] J.J. Lewandowski, M. Seifi, Metal Additive Manufacturing: A Review of Mechanical Properties, Annu. Rev. Mater. Res. 46 (2016) 151–186. doi:10.1146/annurev-matsci-070115-032024.

[151] I. Tolosa, F. Garciandía, F. Zubiri, F. Zapirain, A. Esnaola, Study of mechanical properties of AISI 316 stainless steel processed by "selective laser melting", following different manufacturing strategies, Int. J. Adv. Manuf. Technol. 51 (2010) 639–647. doi:10.1007/s00170-010-2631-5.

[152] I. Yadroitsev, M. Pavlov, P. Bertrand, I. Smurov, Mechanical properties of samples fabricated by selective laser melting, 14èmes Assises Eur. Du Prototypage Fabr. Rapide. 625 (2009) 24–25.

[153] W.E. Luecke, J.A. Slotwinski, Mechanical Properties of Austenitic Stainless Steel Made by Additive Manufacturing, J. Res. Natl. Inst. Stand. Technol. 119 (2014) 398. doi:10.6028/jres.119.015.

[154] J. Delgado, J. Ciurana, C.A. Rodríguez, Influence of process parameters on part quality and mechanical properties for DMLS and SLM with iron-based materials, in: Int. J. Adv. Manuf. Technol., 2012: pp. 601–610. doi:10.1007/s00170-011-3643-5.

[155] B. Zhang, L. Dembinski, C. Coddet, The study of the laser parameters and environment variables effect on mechanical properties of high compact parts elaborated by selective laser melting 316L powder, Mater. Sci. Eng. A. 584 (2013) 21–31. doi:10.1016/j.msea.2013.06.055.

[156] A. Laohaprapanon, P. Jeamwatthanachai, M. Wongcumchang, N. Chantarapanich, S. Chantaweroad, K. Sitthiseripratip, S. Wisutmethangoon, Optimal scanning condition of selective laser melting processing with stainless steel 316L powder, 2011 2nd Int. Conf. Mater. Manuf. Technol. ICMMT 2011, July 8, 2011 - July 11, 2011. 341–342 (2012) 816–820. doi:10.4028/www.scientific.net/AMR.341-342.816.

[157] A. Röttger, K. Geenen, M. Windmann, F. Binner, W. Theisen, Comparison of microstructure and mechanical properties of 316 L austenitic steel processed by selective laser melting with hot-isostatic pressed and cast material, Mater. Sci. Eng. A. 678 (2016) 365–376. doi:10.1016/j.msea.2016.10.012.

[158] M. Averyanova, P. Bertrand, B. Verquin, Effect of initial powder properties on final microstructure and mechanical properties of parts manufactured by selective laser melting, Ann. DAAAM Proc. Int. DAAAM Symp. 21 (2010) 1531–1532. http://www.engineeringvillage.com/blog/document.url?mid=cpx_b784c2d1478e720776M4b8d10178163125&database=cpx.

[159] K. Dalgarno, Materials research to support high performance RM parts, in: Rapid Manuf. 2nd Int. Conf. Loughbrgh. Univ., 2007: pp. 147–56.

[160] G. Strano, L. Hao, R.M. Everson, K.E. Evans, A new approach to the design and optimisation of support structures in additive manufacturing, Int. J. Adv. Manuf. Technol. 66 (2013) 1247–1254. doi:10.1007/s00170-012-4403-x.

[161] K. Mumtaz, N. Hopkinson, Top surface and side roughness of Inconel 625 parts processed using selective laser melting, Rapid Prototyp. J. 15 (2009) 96–103. doi:10.1108/13552540910943397.

[162] M. Badrossamay, T.H.C. Childs, Layer Formation Studies in Selective Laser Melting of Steel Powders, Int. Solid Free. Fabr. Symp. (2006) 268–279.

[163] B. Vandenbroucke, J.-P. Kruth, Selective laser melting of biocompatible metals for rapid manufacturing of medical parts, Rapid Prototyp. J. 13 (2007) 196–203. doi:10.1108/13552540710776142.

[164] J.-P. Kruth, B. Vandenbroucke, J. Van Vaerenbergh, I. Naert, Rapid Manufacturing of Dental Prostheses by means of Selective Laser Sintering / Melting, J. Dent. Technol. (2007) 24–32.

[165] D. Dai, D. Gu, Effect of metal vaporization behavior on keyhole-mode surface morphology of selective laser melted composites using different protective atmospheres, Appl. Surf. Sci. 355 (2015) 310–319. doi:10.1016/j.apsusc.2015.07.044.

[166] D. Wang, Y. Liu, Y. Yang, D. Xiao, Theoretical and experimental study on surface roughness of 316L stainless steel metal parts obtained through selective laser melting, Rapid Prototyp. J. 22 (2016) 706–716. doi:10.1108/RPJ-06-2015-0078.

[167] M. Jamshidinia, R. Kovacevic, The influence of heat accumulation on the surface roughness in powder-bed additive manufacturing, Surf. Topogr. Metrol. Prop. 3 (2015) 14003. doi:10.1088/2051-672X/3/1/014003.